UNIVERSITÀ DEGLI STUDI DI TRENTO

DEPARTMENT OF PHYSICS

Ph.D. Thesis in Physics

A Quantum Monte Carlo approach to dark matter-nuclei interaction

Supervisor:
Prof. Francesco Pederiva

Candidate:
Lorenzo Andreoli
XXXI Cycle

July 18, 2019

[. . .] If this should be verified, it
would lead to the surprising result
that dark matter exists in much
greater density than luminous matter.

FRITZ ZWICKY — 1933

Contents

List of Figures

List of Tables

Abstract

Using quantum Monte Carlo Methods, we compute the differential cross sections for elastic scattering of dark matter (DM) particles off light nuclei, up to $A = 6$ (d, ^{3}H, ^{3}He, ^{4}He, and ^{6}Li). DM-nucleon one- and two-body currents are obtained to next-to-leading order in chiral effective theory, and they are derived from a DM-quark and DM-gluon effective interaction. The nuclear ground states wave functions are obtained from a phenomenological nuclear Hamiltonian, composed of the Argonne v_{18} two-body interaction and the three-body Urbana IX. In this framework, we study the impact of one- and two-body currents and discuss the size of nuclear uncertainties. This work evaluates for the first time two-body effects in $A = 4, 6$ systems and provides the nuclear structure input that can be used to assess the sensitivity of future experimental searches of (light) dark matter, especially relevant for possible experimental targets such as ^{3}He and ^{4}He.

Acronyms

BBN big bang nucleosynthesis
BSM beyond standard model
CD charge dependent
CDM cold dark matter
CI charge independent
CMB cosmic microwave background
CSB charge symmetry breaking
DD direct detection
DM dark matter
DMC diffusion Monte Carlo
EFT effective field theory
LEC low energy constant
LO leading order
NLO next-to-leading-order
N2LO next-to-next-to-leading-order
N3LO next-to-next-to-next-to-leading-order
NR non-relativistic
OPE one pion exchange
QCD quantum chromodynamics
QMC quantum Monte Carlo
SM standard model
VMC variational Monte Carlo
WIMP weakly interactive massive particle

χ**PT** chiral perturbation theory

Introduction

One of the main open problems in physics is understanding the matter and energy content of our universe and their origin. Present accurate data [1], coming from the Wilkinson microwave anisotropy probe (WMAP), shows that the universe is composed of only 4.6% ordinary, baryonic matter. Most of the mass is in the form of dark energy (71.4%), and 24% is non-relativistic, non-baryonic, dark matter (DM).

The nature of DM is unknown, and the scientific community has dedicated many efforts and resources to dark matter searches. Unfortunately, searches for a DM signal from direct, indirect, and accelerator experiments have not yet been successful and all current evidence for DM existence, though extremely strong, only comes from astrophysics and cosmology.

Despite its incredible successes, the Standard Model (SM) cannot explain the existence of DM. Nonetheless, particle physics plays a vital role in this search, proposing theories beyond the standard model (BSM) that include a new, or multiple, types of elementary particles. Many candidates have been proposed over the years [2, 3], however, with time commonalities started to emerge, especially regarding mass and cross section of the particle species considered. For DM to be a cold relic, for example, its mass cannot be lighter

than $1 - 100$ keV [2]. In addition, to reproduce the dark matter density in our universe, the DM particle self-annihilation cross section has to be around the weak scale.

A promising class of these candidates falls under the description of weakly interactive massive particles (WIMP). This kind of particle is, as the name suggests, massive (with a mass usually ranging from the GeV to TeV scale) and interacts only via gravitational and weak force. WIMPs have motivated many experiments, in direct detection searches, aimed at measuring DM signals via nuclear recoils.

Though the majority of these experiments use heavy nuclei, there is a growing interest in using light nuclei to extend the range of DM mass to the sub-GeV scale [4].

In this thesis, we focus on attempting a prediction of the cross section for DM scattering off a variety of light nuclei, namely d, ^{3}H, ^{3}He, ^{4}He and ^{6}Li. Light nuclei are interesting for both theoretical and experimental reasons. In direct detection experiments, light nuclear masses (helium is a promising target candidate [5–9], also for directional detection [10]) offer better a kinematic match to light DM particles; the sensitivity of existing experiments, that use heavy nuclei as targets, decreases sharply for DM masses below 1 GeV. In addition, accurate ab initio nuclear calculations can be performed for the mentioned light nuclei.

In the framework of effective field theory (EFT), we start from DM-quark and DM-gluon interactions and derive DM-nucleons interactions using chiral EFT. The interactions are then used together with quantum Monte Carlo (QMC) nuclear calculations, to compute the matrix elements and total

cross section for elastic scattering off the nuclei mentioned above. Especially relevant for this work, MC methods have been used in recent years to study the impact of two body currents, in β decays [11], electron scattering [12, 13] and neutral-current neutrino scattering [13, 14].

This approach allows for a direct match of cross sections to the interaction at high energy scales and could provide the nuclear input needed in the interpretation of future experimental searches, in the case of ^{3}He and ^{4}He. Our calculations can give the differential cross section and event rate for DM-nucleus elastic scattering, for any arbitrary set of Wilson coefficients in the effective high energy Lagrangian, that in turn can be determined in particular models for the interaction.

The present work is organized as follows:

In **Chapter 1** we briefly introduce dark matter and its experimental evidence, the WIMP paradigm, and the main present and future efforts in direct detection searches that use light nuclei as potential targets.

In **Chapter 2** we present the effective Lagrangian for the interaction between DM-quarks and DM-gluons. We summarize the derivation of DM-nucleon interaction using chiral perturbation theory and present the one-and two body current, up to next-to-leading-order (NLO) in the chiral expansion, for the case of scalar interaction.

In **Chapter 3** the variational Monte Carlo (VMC) method used to perform nuclear calculations is presented. We give a detailed description of the nuclear Hamiltonian and the accurate wave functions used in the VMC.

In **Chapter 4** we present the results for elastic scattering cross section

and the relative contribution of the currents arising at NLO, i.e. radius and two body correction.

In **Chapter 5** we present the conclusions of our work and discuss future perspectives.

Chapter 1

Dark matter

In the elusive quest of detecting DM and shedding light on its nature, many candidates and mechanisms have been proposed (Fig. 1.1). In the last three decades, the main and long-standing paradigm is that DM is mostly cold, and made up of non-baryonic particles not included in the standard model. The modern Lambda-CDM model can account for how our universe went from a very smooth initial state (where fluctuations were extremely small, as can be seen from the cosmic microwave background), to the large-scale structure of galaxies and clusters of galaxies, as observed at present times. Inside this model, many candidates have been proposed over the years, to account for the observed relic density of dark matter.

In this Chapter, we will summarize the main evidence for DM, present the class of DM particles that go under the name of WIMPs, weakly interacting massive particles, and their direct detection. While past and present experiments in direct detection use heavy nuclei as targets, we will focus on the main motivations for using light nuclei, on which we base this work.

1.1 Evidence for dark matter

We briefly outline the main cosmological and astrophysical evidence for the existence of dark matter in our universe:

- Motion of galaxies — Historically, the presence of non-luminous matter in the universe was proposed to explain the discrepancy between the motion of galaxies and the visible mass, deduced from the measure of luminosity. The observed mass was not sufficient to keep the system gravitationally bound. F. Zwicky was one of the first to infer, in 1933, that most of the matter in galaxy clusters is dark. He based his conclusion on the velocity distribution of galaxies in the Coma cluster.

- Large scale structure — Our universe exhibits structure, at scales of fractions to the size of the observable universe, like galaxy superclusters, filaments, and voids. It seems that it is not possible to reproduce the evolution of observed structure in numerical simulations, without accounting for the dark matter content of our universe.

- Galaxy rotation curves – The observed stellar rotational velocity, in galaxies, is roughly constant as the distance from the galactic center increases. This result is in apparent contradiction with Newton's law of gravity, that would instead predict a decrease in radial velocities. Dark matter can account for the observations, if we postulate that it is distributed around each galaxy, forming a spherical halo.

- Gravitational lensing – Since massive objects deflect light, the gravitational lensing effect can be used to derive the total mass contained

in an observed region. A famous measurement is given by the Bullet Cluster [15], consisting of two separated galaxy clusters, merging into a bigger one. It was found that the visible mass of this system only accounts for 2% of its total mass, so dark matter is needed to explain the discrepancy.

- Cosmic Microwave Background (CMB) – The CMB gives information, among others, about the total matter-energy content of our universe, and the percentage of baryonic matter in our universe. The most recent data from WMAP shows that only approximately 4.6% of the total mass/energy of the universe is in the form of ordinary, baryonic matter. The rest is in the form of dark matter and dark energy.

- Big Bang Nucleosynthesis (BBN) – The standard model of BBN explains how, in the time of the universe from 0.1s to 10^4s, the bulk of the observed ^{4}He and ^{2}H, as well as ^{3}He and ^{6}Li, were produced. Historically, BBN was used to estimate the fractional contribution of baryons to the critical density of the universe and can be used to constrain properties and production mechanisms of DM particles.

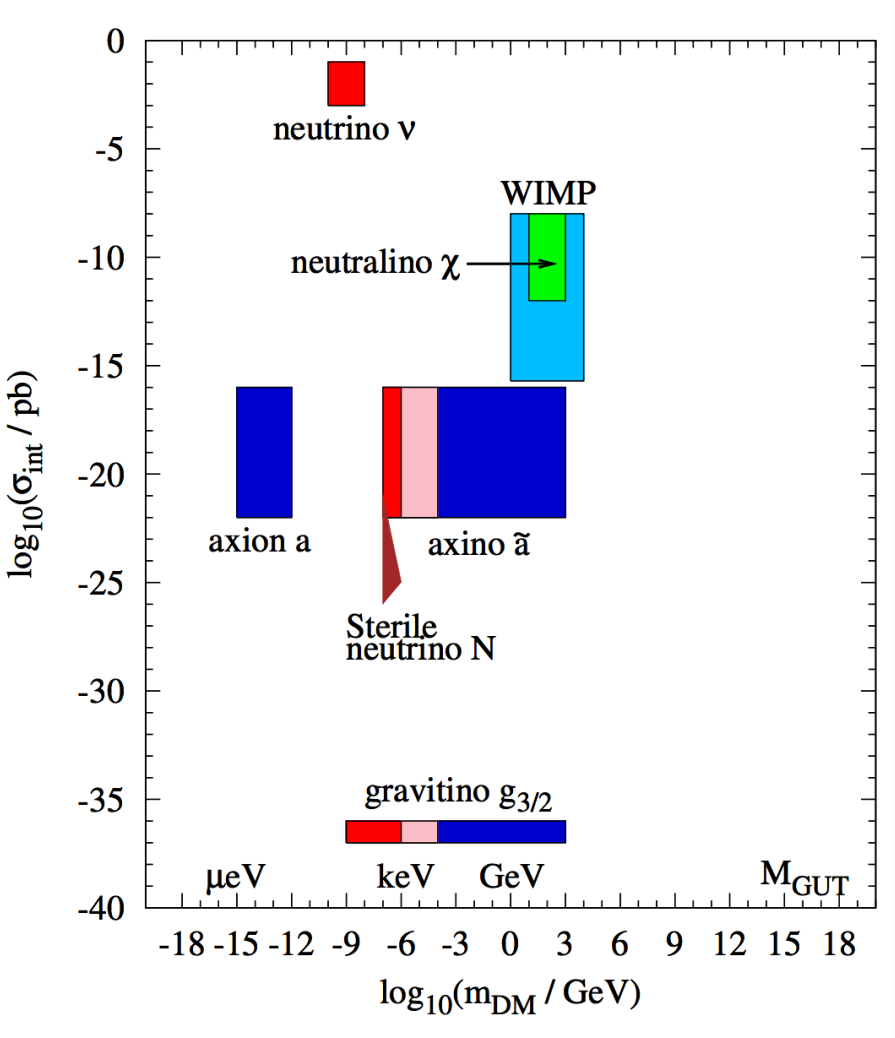

Figure 1.1: Overview of dark matter candidates, as a function of mass and cross section. Figure taken from [3].

1.2 Weakly Interactive Massive Particle

WIPMs, in the form of non-baryonic cold DM, have been one of the leading paradigms in dark matter for many decades [2]. Their motivation initially originated by the so-called "wimp miracle". Starting with a full thermal and chemical equilibrium between DM and SM particles, in the very early universe, WIMPs eventually froze out of equilibrium as the universe expanded. DM particles ceased to annihilate, when their annihilation rate Γ became less than the expansion rate of the universe H:

$$\Gamma = n_\chi \langle \sigma_{\text{ann}} v \rangle \lesssim H, \tag{1.1}$$

where n_χ is the DM particles number density, σ_{ann} the pair annihilation cross section, v the relative velocity, and $\langle\rangle$ denotes a thermal average. Surprisingly, one obtains the correct density of $\Omega_\chi h^2 = 0.12$ [16] if

$$\langle \sigma_{\text{ann}} v \rangle \approx 3 \times 10^{-26} \text{cm}^3/\text{s}, \tag{1.2}$$

which in turn gives a cross section that would arise from a weak interaction, for typical non-relativistic values of v. This would be the case, for example, of a neutrino with a mass of several GeV annihilating through a Z boson exchange.

While DM candidates span many orders of magnitude both in mass and cross section, as can be seen in Fig. 1.1, WIMPs occupy a convenient region in the parameter space, as they could in principle be detected in various ways. In general, three different strategies are available in experimental searches of

WIMPs (schematically represented in Fig. 1.2, according to the direction of the time axis for the interaction between DM and SM particles):

- Direct Detection, based on the observation of elastic scattering of WIMPs off nuclei, and the measure of the corresponding recoil energies. This is typically done in deep underground detectors, as the backgrounds in this kind of experiments are mostly given by cosmic ray muons and radioactivity.

- Indirect Detection, the detection of annihilation or decay products. Current searches focus mainly on antimatter, photons, and neutrinos, and can be used to constrain the value of DM self-annihilation cross section.

- Collider searches, that aim to measure a missing momentum caused by DM particles leaving the detector. They are done for the most part at the Large Hadron Collider.

1.3 Direct Detection: a case for light nuclei

Experimental efforts aimed at detecting WIMPs through their interaction with nuclei have been focused on heavy nuclei such as Ge and Xe, for the spin-independent case; in this case, the total cross section scales roughly as the square of the mass of the nucleus, due to coherence effects. Heavy nuclei are natural targets for DM particle candidates with masses from 10s of GeV to TeV, and the sensitivity is best for $m_\chi \sim m_N$.

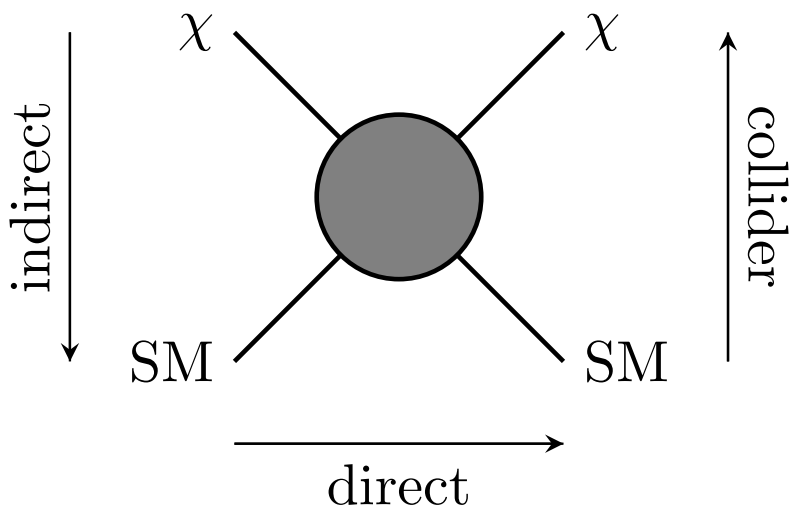

Figure 1.2: Handles on DM detection. Different detection channels, according to the time axis direction. SM indicates Standard Model particles, χ DM particle.

As the sensitivity of direct detection experiment increased (as shown in Fig. 1.3 for spin-independent DM-nucleon cross section), many regions of the mass-cross section parameter space were ruled out. Nonetheless, the sensitivity is significantly reduced both in the high-mass and low-mass regimes.

The interaction rates depend on the interaction cross section, times the WIMP flux at our position in the galaxy. The flux is determined by the local density of DM of 0.39 GeV/cm^3 and its velocity. As the local density is fixed, the flux decreases as $\propto 1/m_\chi$ as the mass increases. On the other hand, the sensitivity of current experiments sharply degrades for light nuclei. The main technical challenge in direct detection experiments come from the smallness of the recoil energy. Considering a DM particle scattering of a nucleus, energy

and momentum conservation limit the maximum recoil energy:

$$E_{\mathrm{R}} = \frac{q^2}{2m_N} \leq \frac{2\mu_{\chi N}^2 v_\chi^2}{m_N}, \tag{1.3}$$

where μ is the reduced mass of the DM-nucleon system.

In fact, the kinematic mismatch between the target mass and DM mass makes the total exchanged momentum and recoil energy too low to be measured, if DM is light.

This is the motivation for the recent interest in alternative strategies for DM direct detection [4], that aim to detect sub-GeV DM particles, using light nuclei.

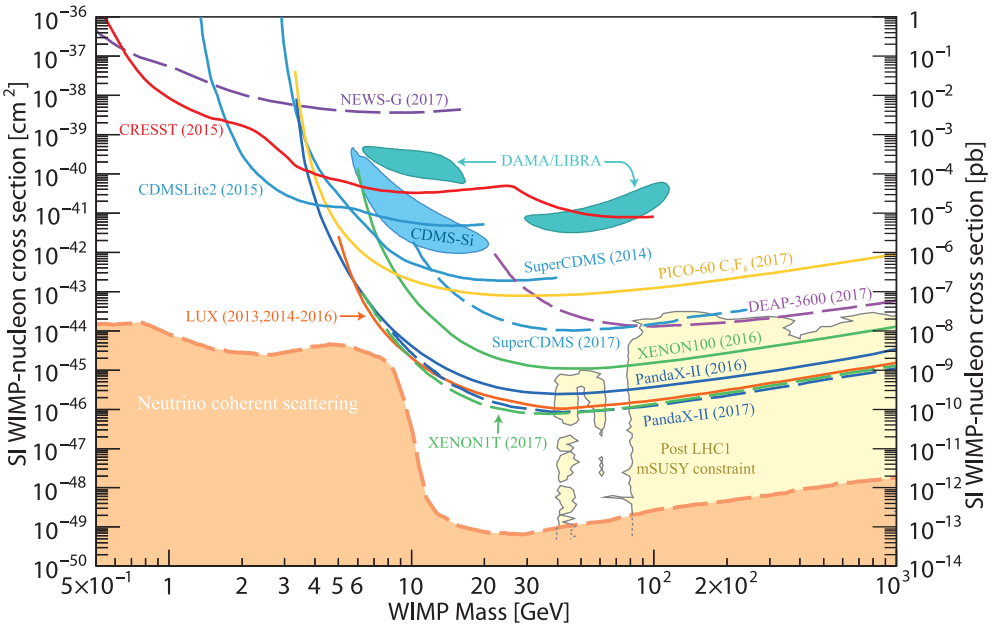

Figure 1.3: Experimental limits for WIMP spin-independent scattering cross section. Figure taken from [17].

An interesting class of proposed experiments focus on Helium as a nuclear target [5–9]. In particular, superfluid ^{4}He is a promising candidate as it

has a relatively good kinematic match to light DM, compared to Xe and Ge. It also has different signal channels: the recoil energy can be detected through the excitation of quasiparticles like phonons and rotons, and these excitations are long-lived and maintain information about recoils. A recently proposed experiment that exploits the favorable features of superfluid ^{4}He with calorimetric readout, presented in [9], could already probe dark matter masses as low as 60 MeV.

Chapter 2

Interaction

It is an interesting feature of nature, that apparently there is interesting physics at all scales: from the age of the universe to the lifespan of a Z boson, from the size of galaxies to nuclei. It is also a fortunate fact of life that we can often neglect what happens at most scales and concentrate on those relevant for the physical phenomena we are interested in.

In principle, if we had a *fundamental* theory, we could "simply" solve it and calculate any quantity we are interested in. In practice that is often impossible, as for example is the case of QCD. Even when it is possible, it is usually not necessary. Intuitively, studying physical quantities that are very small or very large compared to some parameter, we can get an approximate description of the physics simply neglecting the small parameters and effectively consider the large ones as infinite. The subleading effect can then be considered as a small perturbation around our approximation.

The approach described is known as an effective theory (ET), historically it has served physics and physicists well and it has been systematized in

recent decades, especially in the application to effective quantum field theory (QFT). ETs are also extremely useful when the physics is unknown at some scale much higher than the one we are interested in.

In this work, this tool is used to both build an effective interaction for beyond standard model physics, including dark matter in our case, and in the context of chiral perturbation theory (χPT) to derive a DM-nucleon interaction.

The approach used is the following: starting from DM-quark and DM-gluon effective interactions, we derive non-relativistic (NR) interactions for DM-nucleon in the framework of chiral EFT [18–24]. These interactions can be used in ab initio nuclear calculations for few- and many-body systems. This allows us to match the (unknown) physics beyond the standard model, to our calculations for nuclear cross section and, more generally, to the phenomenology of direct, indirect, and collider DM searches.

Several approaches have been used to address the problem of studying the physics of DM-nucleus interactions, and they are based on the possible, different choices of the degrees of freedom of the system. In a top-down order, here are examples of the main approaches to the problem at hand:

- non-relativistic DM-nucleus interactions [25]. Using a simple NR effective theory, [25] builds a minimal set of operators for spin-dependent and spin-independent interaction between dark matter particles and nuclei. This is the simplest effective theory, that corresponds to many underlying microscopic DM theories, whose small number of operators can be tested in direct detection experiments.

- non-relativistic DM-nucleon interactions [26]. Deriving all possible Galilean-invariant operators for the interaction of dark matter and nucleons (up to second order in the exchanged momentum), Fitzpatrick et al. performed shell-model calculations of nuclear responses for a variety of nuclear targets;

- non-relativistic DM-nucleon interactions derived from DM-quark and DM-gluon effective interactions [23, 27]. This is the approach adopted in the present work;

- first-principle, lattice-QCD calculations of matrix elements, for scalar, axial, and tensor currents [28, 29].

In this chapter, we first present an effective Lagrangian for the interaction of DM with quarks and gluons. Focusing then on the scalar case, we briefly summarize the chiral expansion of DM-pion and DM-nucleon interactions and introduce a power counting to identify the leading contributions. Finally, we present the one- and two-body currents for isoscalar and isovector DM-nucleon interaction, up to NLO.

2.1 Effective Lagrangian

Considering the interaction between DM and standard model particles, we make minimal assumptions on its nature and its coupling to the SM. We can build a model-independent interaction, where we extend the SM to include a DM particle as an additional degree of freedom (see Ref. [24]). Introducing a new energy scale $\tilde{\Lambda}$, related to the mass of the mediator or a new interaction

mechanism, BSM physics can be incorporated into a set effective operators organized according to their dimension. In our case, $\tilde{\Lambda}$ is taken to be an energy scale above the QCD scale of about 1 GeV. Such an EFT can in turn model physics at much higher energy, beyond the electroweak scale.
The operators considered in the context of dark matter effective theories have dimension greater than 4 and usually vary in the range from dimension 5, which is the case of Higgs portal DM, to dimension 7[24, 30]. The total number of all possible dimension 6 and 7 effective operators relevant in the context of DM direct detection is quite large. A review can be found in Ref. [31].

Here we only give an example of how an EFT can be built, only considering a small subset of dimension 6 and 7 operators, suppressed by $\tilde{\Lambda}^2$ and $\tilde{\Lambda}^3$ respectively, and take them to have the following form:

$$\mathcal{O} = \bar{\chi}\Gamma_\chi\chi\bar{\psi}\Gamma_\psi\psi, \tag{2.1}$$

with Dirac bilinears $\Gamma_{\chi/\psi} \in \{\mathbb{1}, \gamma^5, \gamma^\mu, \gamma^\mu\gamma^5, \sigma^{\mu\nu}\}$, DM fields χ and $\bar{\chi}$, and quark fields ψ and $\bar{\psi}$. We assume that the DM particle is a spin-1/2 Dirac fermion, such as the neutralino (for the scalar interaction we are interested in, the extension to scalar, vector or Majorana DM particles is straightforward).

The general form of the effective Lagrangian commonly used for DM-quark and DM-gluon includes the possible combination of Dirac bilinears that give rise to scalar (S), pseudoscalar (P), vector (V), axial-vector (A)

and tensor (T) interaction. It has the following form:

$$\mathcal{L}_{\text{eff}} = \mathcal{L}_{\text{S}} + \mathcal{L}_{\text{P}} + \mathcal{L}_{\text{V}} + \mathcal{L}_{\text{A}} + \mathcal{L}_{\text{T}} + \mathcal{L}_{\text{G}}, \tag{2.2}$$

where

$$\mathcal{L}_{\text{S}} = \frac{1}{\tilde{\Lambda}^3} \sum_q \left[c_q^{SS} \bar{\chi}\chi m_q \bar{q}q + c_q^{PS} \bar{\chi} i\gamma^5 \chi m_q \bar{q}q \right], \tag{2.3}$$

$$\mathcal{L}_{\text{P}} = \frac{1}{\tilde{\Lambda}^3} \sum_q \left[c_q^{SP} \bar{\chi}\chi m_q \bar{q} i\gamma^5 q + c_q^{PP} \bar{\chi} i\gamma^5 \chi m_q \bar{q} i\gamma^5 q \right], \tag{2.4}$$

$$\mathcal{L}_{\text{V}} = \frac{1}{\tilde{\Lambda}^2} \sum_q \left[c_q^{VV} \bar{\chi}\gamma^\mu \chi \bar{q}\gamma_\mu q + c_q^{AV} \bar{\chi}\gamma^\mu \gamma^5 \chi \bar{q}\gamma_\mu q \right], \tag{2.5}$$

$$\mathcal{L}_{\text{A}} = \frac{1}{\tilde{\Lambda}^2} \sum_q \left[+ c_q^{VA} \bar{\chi}\gamma^\mu \chi \bar{q}\gamma_\mu \gamma^5 q + c_q^{AA} \bar{\chi}\gamma^\mu \gamma^5 \chi \bar{q}\gamma_\mu \gamma^5 q \right], \tag{2.6}$$

$$\mathcal{L}_{\text{T}} = \frac{1}{\tilde{\Lambda}^2} \sum_q \left[c_q^{TT} \bar{\chi}\sigma^{\mu\nu} \chi \bar{q}\sigma_{\mu\nu} q + \tilde{c}_q^{TT} \bar{\chi}\sigma^{\mu\nu} i\gamma^5 \chi \bar{q}\sigma_{\mu\nu} q \right], \tag{2.7}$$

$$\begin{aligned} \mathcal{L}_{\text{G}} = \frac{1}{\tilde{\Lambda}^3} \Big[& c_g^S \bar{\chi}\chi \alpha_S G^a_{\mu\nu} G_a^{\mu\nu} + c_g^P \bar{\chi} i\gamma^5 \chi \alpha_S G^a_{\mu\nu} G_a^{\mu\nu} \\ & + \tilde{c}_g^S \bar{\chi}\chi \alpha_S G^a_{\mu\nu} \tilde{G}_a^{\mu\nu} + \tilde{c}_g^P \bar{\chi} i\gamma^5 \chi \alpha_S G^a_{\mu\nu} \tilde{G}_a^{\mu\nu} \Big]. \end{aligned} \tag{2.8}$$

For convenience, the quark masses are included in the definition of scalar and pseudoscalar operators. The dimensionless Wilson coefficients c_q and c_g are free parameters of the theory and contain all information about short-distance physics above the scale $\tilde{\Lambda}$.

2.2 Scalar interaction

In this section, we focus on the scalar interaction between the DM particle and standard model fields. Scalar interactions arise naturally in many extension of the SM; one notable example is via the exchange of Higgs and squarks [32] (supersymmetric counterpart of a quark) in supersymmetric models, as shown in Fig. 2.1.

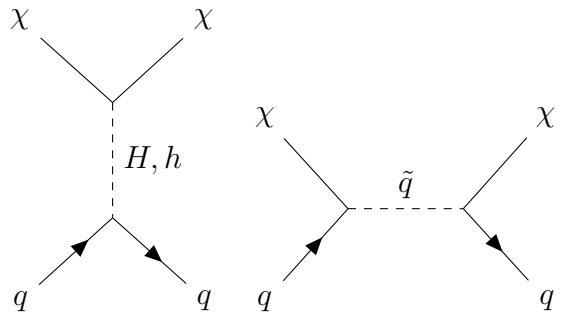

Figure 2.1: Feynman diagrams contributing to spin-independent neutralino-quark scattering.

The scalar case also has the interesting feature that two-body currents appear already at next-to-leading order in the chiral expansion while for the other currents derived from Eq. (2.2), they only appear at higher orders. The effective Lagrangian describing scalar-mediated DM-quark and DM-gluon interactions is built from dimension-7 operators [19] and is contained in Eq. (2.2) (for convenience of notation, we drop the labels SS, S in the Wilson coefficients):

$$\mathcal{L}^{S}_{\text{eff}} = \frac{1}{\tilde{\Lambda}^3}\left(\sum_{q=u,d,s} c_q \bar{\chi}\chi m_q \bar{q}q + c_G \bar{\chi}\chi \alpha_s G^a_{\mu\nu} G^{\mu\nu}_a\right), \tag{2.9}$$

where we only consider light quark field q, α_s is the strong coupling constant,

and $G_{\mu\nu}$ is the gluon field strength tensor.

We now need to match this scalar Lagrangian to a DM-nucleon effective interaction, non-perturbatively, at an energy scale corresponding to the chiral-symmetry-breaking scale of ~ 1 GeV. In order to do that we use chiral perturbation theory [33–35], the effective theory that allows us to study the low-energy dynamics of QCD. χPT is a powerful tool that encapsulate the non-perturbative nature of QCD into a set of low energy constants (LECs), that can be determined from experimental data or calculated using lattice QCD.

In this work we will focus mainly on the isoscalar and isovector DM-quark interactions, derived in the context of SU(2) χPT, following the derivation in [23, 36]. The full SU(3) derivation can be found in [19]. While we do not account for the effect of strange bosons, that require SU(3) χPT, we will briefly comment on their effect in Chapter 4.

The scalar terms in Eq. (2.9) break the chiral symmetry of QCD in the same way as the quark masses do. The external scalar source can then be included using the spurion trick, as in ordinary chiral perturbation theory, where the mass matrix $\mathcal{M}$ is replaced by

$$\begin{pmatrix} m_u(1 - c_u/\tilde{\Lambda}^3\bar{\chi}\chi) & 0 \\ 0 & m_d(1 - c_d/\tilde{\Lambda}^3\bar{\chi}\chi) \end{pmatrix}. \tag{2.10}$$

At the level of pions and nucleons, the interactions become

$$\mathcal{L}^{\pi}_{\chi,q} = \frac{c^{\pi}_q}{\tilde{\Lambda}^3}\boldsymbol{\pi}^2\bar{\chi}\chi, \tag{2.11}$$

$$\mathcal{L}_{\chi,N} = \frac{c_{\rm is}^N}{\tilde{\Lambda}^3}\bar{N}N\bar{\chi}\chi + \frac{c_{\rm iv}^N}{\tilde{\Lambda}^3}\bar{N}\tau^3 N\bar{\chi}\chi, \tag{2.12}$$

where we have introduced pion and nucleon fields.

$$c_q^\pi = \frac{m_\pi^2}{2}\frac{c_u m_u + c_d m_d}{m_u + m_d} \equiv \frac{m_\pi^2}{2}c_{\rm is} \tag{2.13}$$

$$c_{\rm is}^N = -4m_\pi^2 c_1 c_{\rm is} \tag{2.14}$$

$$c_{\rm iv}^N = B\left(m_d - m_u\right)c_5 2\frac{c_d m_d - c_u m_u}{m_d - m_u} \equiv B\left(m_d - m_u\right)c_5 c_{\rm iv} \tag{2.15}$$

The low energy constants c_1 and c_5 are related to the nucleon σ term and strong proton-neutron mass splitting, respectively. Eq. (2.13) and Eq. (2.15) define the effective isoscalar and isovector couplings, linear combinations of c_u and c_d Wilson coefficients.

The maximum momentum transfer in elastic scattering between DM and light nuclei, as shown in Eq. (4.5), is of the order of tens of MeV, small compared to the chiral-symmetry-breaking scale. For simplicity, we will consider it the same as typical nuclear binding momentum $p \sim m_\pi$, and introduce a power counting scheme, to order in powers of p/Λ_χ the possible diagrams that can be constructed out of DM-pions and DM-nucleons interactions in Eq. (2.11) and Eq. (2.12). We use the standard χPT power counting for irreducible diagrams, which is the following:

- $p^4/(4\pi)^2$ for each loop,

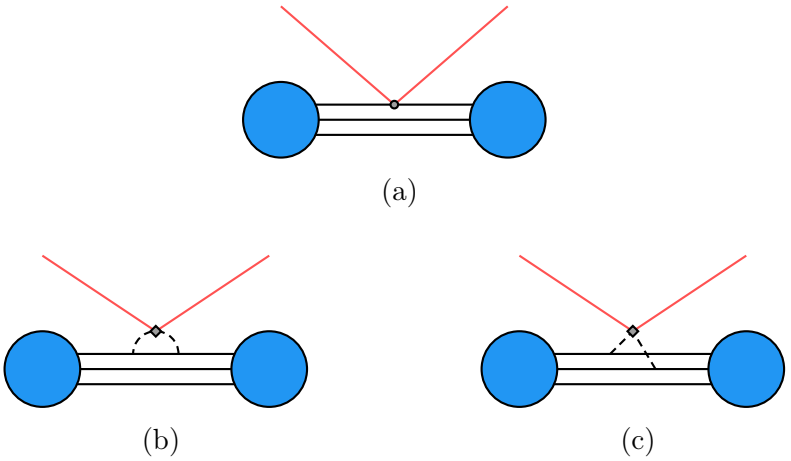

Figure 2.2: Diagrams contributing to DM-nucleus scattering up to NLO. Solid black lines denote nucleons; dashed lines denote pions. (a) Leading order interaction. (b) One-body NLO interaction. (c) Two-body NLO interaction.

- $1/p$ for each nucleon propagator,
- $1/p^2$ for each pion propagator.

For reducible diagrams in Fig. 2.2, that only contain nucleon propagators, the above power counting needs to be modified, as first shown by Weinberg [37–39]. In those diagrams, the nucleon energy becomes of $\mathcal{O}(p^2/m_N)$. We then replace, in those diagrams, one power or p with $p \to p^2/m_N$. This way, the nucleon propagator becomes m_N/p and loops scale as $p^5/((4\pi)^2 m_N)$.

With this counting scheme, the diagrams contributing up to NLO are shown in Fig. 2.2. Fig. 2.2a is the LO interaction, while Figs. 2.2b and 2.2c are one- and two-body NLO interactions, respectively.

We now finally present the expression for one- and two-body currents, at the nucleon level. In Fig. 2.3, we denote with $\boldsymbol{p}_i$ and $\boldsymbol{k}$ ($\boldsymbol{p}_i'$ and $\boldsymbol{k}'$) incoming (outgoing) momenta, respectively for nucleons and DM particles.

The exchanged momentum is $\boldsymbol{q} = \boldsymbol{k}' - \boldsymbol{k} = \boldsymbol{p}_i - \boldsymbol{p}'_i$.

With this convention for momenta, the elastic scattering is schematically

$$N(\boldsymbol{p}_i) + \chi(\boldsymbol{k}) \to N(\boldsymbol{p}'_i) + \chi(\boldsymbol{k}'), \tag{2.16}$$

where the index i refers to the ith nucleon.

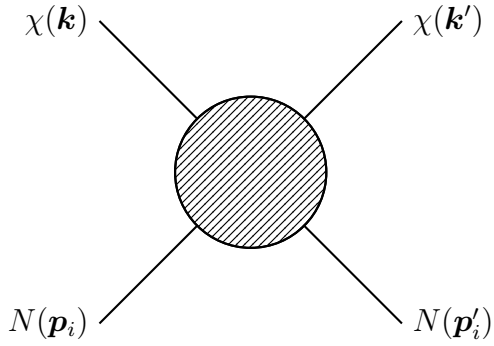

Figure 2.3: Schematics of DM-nucleon scattering. The time direction goes from left to right, with primed momenta denote outgoing particles. N indicates nucleons, χ indicates DM particles.

With the definition of isoscalar and isovector effective couplings, the momentum space expressions for the one-body current is:

$$J^{(1)}(\boldsymbol{q}_i) = \frac{c_{\rm is}}{\tilde{\Lambda}^3}\left[\sigma_{\pi N} - \frac{9g_A^2\pi m_\pi^3}{4(4\pi f_\pi)^2}F\left(\frac{|\boldsymbol{q}_i|}{2m_\pi}\right)\right] - \frac{c_{\rm iv}}{\tilde{\Lambda}^3}\frac{\delta m_N}{4}\tau_i^z \tag{2.17}$$

$$F(x) = \frac{-x + (1+2x^2)\arctan x}{3x}, \tag{2.18}$$

where $\sigma_{\pi N} = \frac{m_u+m_d}{2}\langle p|\bar{u}u + \bar{d}d|p\rangle$ is the nucleon σ term and $\delta m_N = (m_n - m_p)_{\rm strong}$ the strong mass splitting, that constitute the LO one-body contribution. Their numerical values used in this work are taken from Refs. [40] (obtained from a Roy-Steiner analysis of pion-nucleon scattering)

and [41]. They are, respectively,

$$\sigma_{\pi N} = (59.1 \pm 3.5)\ \text{MeV}, \quad \delta m_N = (2.32 \pm 0.17)\ \text{MeV}\,. \tag{2.19}$$

The momentum dependent part of Eq. (2.17) appears at NLO, and for small exchanged momenta is proportional to $F(|\boldsymbol{q}_i|/2m_\pi \sim \boldsymbol{q}_i^2|/4m_\pi^2$.

Its size, relative to the leading order, depends on the choice of the σ term and our numerical results can be easily extended to other values coming, for example, from lattice QCD calculations [42].

The two-body current, also appearing at NLO (Fig. 2.2c), is given by

$$J^{(2)}_{\pi\pi}(\boldsymbol{q}_i, \boldsymbol{q}_j) = -\frac{c_{\text{is}}}{\tilde{\Lambda}^3}\left(\frac{g_A}{2F_\pi}\right)^2 m_\pi^2 \boldsymbol{\tau}_i \cdot \boldsymbol{\tau}_j \frac{\boldsymbol{\sigma}_i \cdot \boldsymbol{q}_i \boldsymbol{\sigma}_j \cdot \boldsymbol{q}_j}{(\boldsymbol{q}_i^2 + m_\pi^2)(\boldsymbol{q}_j^2 + m_\pi^2)}\,. \tag{2.20}$$

This currents, once transformed to coordinate space, are used to calculate the differential cross section shown in the next chapter. The sum of one- and two-body currents is:

$$J(\boldsymbol{q}) = \sum_i e^{i\boldsymbol{q}\cdot\boldsymbol{r}_i} J^{(1)}(\boldsymbol{q}) + \sum_{i<j} J^{(2)}_{\pi\pi}(\boldsymbol{q}; \boldsymbol{r}_i, \boldsymbol{r}_j)\ , \tag{2.21}$$

where the expression for the Fourier transform of $J^{(2)}_{\pi\pi}(\boldsymbol{q}_i, \boldsymbol{q}_j)$ is given in the Appendix.

Chapter 3

Method

In this work, we are interested in the nuclear aspects of DM elastic scattering. In order to calculate the differential cross sections for this process, we need to choose an interaction between the nucleons, and a method to calculate the relevant matrix elements between nuclear states. DM particles are non-relativistic and the maximum energy transferred we consider is less than 100 MeV, much less than the mass of the nucleons and the binding energy of the nuclei. Choosing nucleons as degrees of freedom, instead of quarks and gluons, is then appropriate for the process considered.

In this regime, many-body methods can be used to calculate properties of nuclei and in particular, the standard methods used in nuclear physics have been applied in the context DM-nucleus scattering. For example, in heavy nuclei, state-of-the art shell model calculations have been performed [22, 43], providing the nuclear structure factors relevant for experimental targets.

For lighter systems, with $A < 4$, direct methods can be applied to the solution of the Schrödinger equation. Ref. [23], that is the main work which

we can compare our result to, solves the Faddeev equations for systems with $A = 2, 3$.

In this chapter, we focus on the class of quantum Monte Carlo (QMC) methods, that in recent years have proven to be extremely successful in describing properties of nuclei [44–46], from light to medium-heavy. In particular, we will present the variational Monte Carlo (VMC) method, the phenomenological interaction we adopt for two- and three-nucleon, and the accurate nuclear wave functions used to calculate the differential cross section. We also give the calculated ground state energies E and proton point radii r_p for the nuclei of interest, from d to ^{6}Li.

3.1 Monte Carlo Methods

When considering a system of interacting nucleons, solving the Schrödinger equation is a formidable task. Even considering the simpler problem of calculating expectation values of operators of the form (neglecting for the moment spin and isospin degrees of freedom)

$$\langle \hat{\mathcal{O}} \rangle = \frac{\langle \psi | \hat{\mathcal{O}} | \psi \rangle}{\langle \psi | \psi \rangle} = \frac{\int d\boldsymbol{R} \psi^* \hat{\mathcal{O}} \psi}{\int d\boldsymbol{R} \psi^* \psi} = \int d\boldsymbol{R} \frac{|\psi|^2}{\int d\boldsymbol{R} |\psi|^2} \frac{\hat{\mathcal{O}}\psi}{\psi} \,, \tag{3.1}$$

$$\boldsymbol{R} = \{\boldsymbol{r}_1, \ldots, \boldsymbol{r}_A\} \,, \tag{3.2}$$

naïve integration methods cannot be used in practice, because the numerical error grows exponentially with the dimensionality of the system.

Stochastic integration, on the other hand, allows us to calculate the de-

sired expectation value, provided we can generate configurations $\{\boldsymbol{R}_i\}$, sampled from the normalized and positive-definite probability distribution function

$$f(\boldsymbol{R}) = \frac{|\psi(\boldsymbol{R})|^2}{\int d\boldsymbol{R}|\psi(\boldsymbol{R})|^2}. \tag{3.3}$$

Considering N independent samples, the expectation value in Eq. (3.1) simply becomes

$$\langle\hat{\mathcal{O}}\rangle \simeq \frac{1}{N}\sum_{i=1}^{N}\frac{\hat{O}\psi(\boldsymbol{R}_i)}{\psi(\boldsymbol{R}_i)}. \tag{3.4}$$

Thanks to the central limit theorem [47], if the samples are statistically independent, the numerical error on the estimate of the integral decreases as the inverse square root of the number of samples ($\sigma \sim 1/\sqrt{N}$). The error can in principle be made arbitrary small increasing the computation time.

General purpose methods exist for generating configurations from a given probability distribution function. In this work we adopt the Metropolis algorithm [48], based on the concept of Markov chain, in which one generates sets of configurations $\boldsymbol{R}_i$, each one depending only on the previous one, in such a way that the set of configurations has the desired distribution function f as its equilibrium distribution.

This algorithm follows from a factorization of the transition matrix $\boldsymbol{M}$, used to generate new configurations $\boldsymbol{R}_{i+1}$ starting from $\boldsymbol{R}_i$, into a proposal and acceptance

$$\mathrm{M}\left(\boldsymbol{R}_i, \boldsymbol{R}_{i+1}\right) = \mathrm{T}\left(\boldsymbol{R}_i, \boldsymbol{R}_{i+1}\right)\mathrm{A}\left(\boldsymbol{R}_i, \boldsymbol{R}_{i+1}\right), \tag{3.5}$$

and it produces configurations distributed according to Eq. (3.3), regardless of the specific choice of $\boldsymbol{T}$ and the details of the probability distribution

function.

A constructive way of generating such configurations is iterating the following:

1. From a symmetric proposal $\boldsymbol{T}(\boldsymbol{R}_i, \boldsymbol{R}_{i+1})$, generate a new configuration $\boldsymbol{R}_{i+1}$

2. Calculate the acceptance probability

$$\mathbf{A}\left(\boldsymbol{R}_i, \boldsymbol{R}_{i+1}\right) = \min\left[1, \frac{\mathbf{T}\left(\boldsymbol{R}_i, \boldsymbol{R}_{i+1}\right) f\left(\boldsymbol{R}_{i+1}\right)}{\mathbf{T}\left(\boldsymbol{R}_{i+1}, \boldsymbol{R}_i\right) f(\boldsymbol{R}_i)}\right]$$

3. Accept the new configuration $\boldsymbol{R}_{i+1}$ with probability $\boldsymbol{A}(\boldsymbol{R}_i, \boldsymbol{R}_{i+1})$

   - if $\boldsymbol{A} \geq 1$, accept $\boldsymbol{R}_{i+1}$
   - if $\boldsymbol{A} < 1$, generate a uniform random number $\eta \in [0, 1]$ and accept $\boldsymbol{R}_{i+1}$ if $\eta < \boldsymbol{A}$.

It is also convenient that, in the definitions of the acceptance probability $\boldsymbol{A}$, the normalization in Eq. (3.3) cancels out.

The stochastic integration we presented can be used to evaluate the energy in the case $\hat{\mathcal{O}} = \hat{H}$, together with the variational theorem, to find approximate wave functions for the ground state of the system. This approach is called variational Monte Carlo (VMC).

Constructing a trial wave function $|\psi\rangle$ with embedded variational parameters $\{\alpha_i\}$, one can find the values of the parameters that minimize the energy:

$$E_V = \frac{\langle\psi|\hat{H}|\psi\rangle}{\langle\psi|\psi\rangle}, \tag{3.6}$$

and find a good approximation for the nuclear ground state.

Thanks to the variational principle, the energy of any trial wave function is always greater than that of the ground state, and the equality holds for $|\psi\rangle = |\psi_0\rangle$

This can be easily proven by expanding the trial wave functions on a basis of eigenstates of $\hat{H}$:

$$\hat{H}|\psi_n\rangle = E_n|\psi_n\rangle, \tag{3.7}$$

$$|\psi\rangle = \sum_n c_n|\psi_n\rangle. \tag{3.8}$$

Since $E_n \geq E_0$, we obtain the following inequality:

$$E_V = \frac{\sum_n E_n|c_n|^2}{\sum_n|c_n|^2} \geq \frac{E_0\sum_n|c_n|^2}{\sum_n|c_n|^2} = E_0. \tag{3.9}$$

It is clear that the equality holds only if $c_0 = 1$ and $c_n = 0$ for $n > 0$.

We will now give the details of the phenomenological Hamiltonian and the wave function used in the calculations.

3.2 Nuclear Hamiltonian

Regarding the choice of the interaction between nucleons, we use a non-relativistic nuclear Hamiltonian in configuration-space, consisting of a two-body Argonne v_{18} potential [49], and a three-body Urbana IX potential [50]. The Argonne potential is a local, finite, NN potential, with explicit charge dependence and a complete electromagnetic interaction. We choose to per-

form calculations in coordinate space, since the Argonne potential is one of the most used potential in few and many body nuclear calculations. The VMC calculations could also be a starting point for future diffusion Monte Carlo calculations.

This phenomenological Hamiltonian has been fit to experimental data from the Nijmegen database[51, 52]. It fits both pp and np scattering, low-energy nn scattering and binding energies of light nuclei, with a $\chi^2/N_{\text{data}} \sim 1$, up to energy in the laboratory frame of about 350 MeV.

The total Hamiltonian takes the form

$$\hat{H} = \sum_i \hat{T}_i + \sum_{i<j} \hat{v}_{ij} + \sum_{i<j<k} \hat{v}_{ijk}\,. \tag{3.10}$$

where kinetic energy operator of the ith nucleon is usually written as a sum of charge-independent and charge-symmetry breaking terms, to account for the mass difference between protons and neutrons:

$$\hat{T_i} = -\frac{\hbar^2}{4}\left[\left(\frac{1}{m_p}+\frac{1}{m_n}\right)+\left(\frac{1}{m_p}-\frac{1}{m_n}\right)\tau_i^z\right]\nabla_i^2, \tag{3.11}$$

τ_i^z is the third component of the isospin.

The two-body Argonne v_{18} potential can be written as a sum of 18 operators

$$\hat{v}_{ij} = \sum_{p=1}^{18} v_p\left(r_{ij}\right)\hat{O}_{ij}^p = \hat{v}_{ij}^{\gamma} + \hat{v}_{ij}^{\pi} + \hat{v}_{ij}^{S} + \hat{v}_{ij}^{I} \tag{3.12}$$

which are divided into electromagnetic (EM), a long-range one-pion-exchange (OPE) and phenomenological short- and intermediate-range strong-interaction parts.

The complete EM interaction v_{ij}^{γ} contains Coulomb, Darwin-Foldy, vacuum polarization and magnetic moment terms with finite-size effects, that keep terms finite at $r_{ij} = 0$.

The OPE part has the following structure:

$$\hat{v}_{ij}^{\pi} = f^2 \left[\boldsymbol{X}_{ij} \boldsymbol{\tau}_i \cdot \boldsymbol{\tau}_j + \tilde{\boldsymbol{X}}_{ij} T_{ij} \right]. \tag{3.13}$$

It includes the effect of the mass difference between m_{π^0} and $m_{\pi^\pm}$. The pion-nucleon coupling constant is $f^2 = 0.075$ and the radial functions are (using units $\hbar = c = 1$)

$$\boldsymbol{X}_{ij} = \frac{1}{3} \left(\boldsymbol{X}_{ij}^{0} + 2\boldsymbol{X}_{ij}^{\pm} \right), \tag{3.14}$$

$$\tilde{\boldsymbol{X}}_{ij} = \frac{1}{3} \left(\boldsymbol{X}_{ij}^{0} - \boldsymbol{X}_{ij}^{\pm} \right), \tag{3.15}$$

where

$$\boldsymbol{X}_{ij}^{m} = \left(\frac{m}{m_s} \right)^2 \frac{1}{3} m \left[Y\left(mr_{ij}\right) \boldsymbol{\sigma}_i \cdot \boldsymbol{\sigma}_j + T\left(mr_{ij}\right) S_{ij} \right]. \tag{3.16}$$

$\boldsymbol{\sigma}_i$ and $\boldsymbol{\tau}$ are Pauli matrices operating on the spin and isospin of the nucleons. $S_{ij} = 3\boldsymbol{\sigma}_i \cdot \hat{r}_{ij} \boldsymbol{\sigma}_j \cdot \hat{r}_{ij} - \boldsymbol{\sigma}_i \cdot \boldsymbol{\sigma}_j$ is the tensor operator and $T_{ij} = 3\tau_i^z \tau_j^z - \boldsymbol{\tau}_i \cdot \boldsymbol{\tau}_j$ is the isotensor operator.

The pion and tensor radial functions are the Yukawa and OPE tensor potential, respectively, together with a short-range cutoff of parameter $c = 2.1$ fm^{-1}

$$Y(x) = \frac{e^{-x}}{x} \xi(r), \tag{3.17}$$

$$T(x) = \left(1 + \frac{3}{x} + \frac{3}{x^2}\right) Y(x)\xi(r), \tag{3.18}$$

$$\xi(r) = 1 - \exp\left(-cr^2\right). \tag{3.19}$$

In the region in which r is less than 2 fm, the tensor part dominates the OPE, as $T_\pi(r) \gg Y_\pi(r)$.

The remaining interaction, divided into intermediate- and short-range parts, is composed of 18 operators

$$\hat{v}_{ij}^{I+S} = \hat{v}_{ij}^{I} + \hat{v}_{ij}^{S} = \sum_{p=1}^{18} \left[I^p T^2\left(mr_{ij}\right) + \left(P^p + Q^p r + R^p r^2\right) W(r)\right] \hat{O}_{ij}^p. \tag{3.20}$$

The radial part of the short-range interaction is a quadratic function of r, multiplying a Wood-Saxon potential of radius $r_0 = 0.5$ fm and parameter $a = 0.2$ fm

$$W(r) = \left[1 + e^{(r-r_0)/a}\right]^{-1}. \tag{3.21}$$

I^p, P^p, Q^p and R^p are a set of constants, fitted to the Nijmegen data mentioned above.

Finally, the operators appearing in Eq. (3.20) include 14 charge independent (CI) (they are the same as the Argonne v_{14} potential), 3 charge dependent (CD) and one charge symmetry breaking (CSB) terms.

$$\hat{O}_{ij}^{\mathrm{CI}} = \left[1, \boldsymbol{\sigma}_i \cdot \boldsymbol{\sigma}_j, S_{ij}, \mathbf{L}\cdot\mathbf{S}, \mathbf{L}^2, \mathbf{L}^2\left(\boldsymbol{\sigma}_i \cdot \boldsymbol{\sigma}_j\right), \left(\mathbf{L}\cdot\mathbf{S}\right)^2\right] \otimes \left[1, \boldsymbol{\tau}_i \cdot \boldsymbol{\tau}_j\right] \tag{3.22}$$

$$\hat{O}_{ij}^{\mathrm{CD}} = [1, \boldsymbol{\sigma}_i \cdot \boldsymbol{\sigma}_j, S_{ij}] \otimes T_{ij} \tag{3.23}$$

$$\hat{O}_{ij}^{\mathrm{CSB}} = \tau_i^z + \tau_j^z \tag{3.24}$$

In this expression, $\boldsymbol{L}_{ij}$ is the relative angular momentum of the pair ij and $\boldsymbol{S}_{ij}$ is the total spin of the pair.

$$\boldsymbol{L}_{ij} = \frac{1}{2i} \left(\boldsymbol{r}_i - \boldsymbol{r}_j \right) \times \left(\boldsymbol{\nabla}_i - \boldsymbol{\nabla}_j \right), \tag{3.25}$$

$$\boldsymbol{S}_{ij} = \frac{1}{2} \left(\boldsymbol{\sigma}_i + \boldsymbol{\sigma}_j \right). \tag{3.26}$$

The major contribution to the NN interaction comes from the first 8 terms of Eq. (3.22), as they are necessary to fit S and P wave data in singlet and triplet isospin states.

The three-body NNN Urbana IX is the last of the Urbana series of semi phenomenological potentials [53]. First used together with Argonne v_{18}, this interaction consists of two-pion-exchange and a short-range phenomenological component:

$$\hat{v}_{ijk} = \hat{V}_{ijk}^{2\pi,P} + \hat{V}_{ijk}^{R}. \tag{3.27}$$

The first term, originally introduced by Fujita and Miyazawa [54], is a P-wave component, corresponding to an intermediate excited Δ resonance produced by two-pion exchanges between nucleons $i-j$ and $j-k$. It can be written as a cyclic sum of $\boldsymbol{X}_{ij}$ terms in Eq. (3.16), where the average pion

mass $m = [(1/3)m_{\pi^0} + (2/3)m_{\pi^\pm}]$

$$\begin{aligned}\hat{V}_{ijk}^{2\pi,P} = &\sum_{\text{cyc}} A_{2\pi}^{P} \left\{ \boldsymbol{X}_{ij}^{\pi}, \boldsymbol{X}_{jk}^{\pi} \right\} \left\{ \boldsymbol{\tau}_i \cdot \boldsymbol{\tau}_j, \boldsymbol{\tau}_j \cdot \boldsymbol{\tau}_k \right\} \\ &+ \frac{1}{4} A_{2\pi}^{P} \left[\boldsymbol{X}_{ij}^{\pi}, \boldsymbol{X}_{jk}^{\pi} \right] \left[\boldsymbol{\tau}_i \cdot \boldsymbol{\tau}_j, \boldsymbol{\tau}_j \cdot \boldsymbol{\tau}_k \right] .\end{aligned} \tag{3.28}$$

The remaining term is a central, repulsive phenomenological term, needed to compensate the overbinding in nuclei. Again, it can be expressed as a cyclic sum, in terms of the OPE in Eq. (3.18)

$$\hat{V}_{ijk}^{R} = \sum_{\text{cyc}} A_R T^2 \left(m r_{ij} \right) T^2 \left(m r_{jk} \right) . \tag{3.29}$$

The parameters are fitted to reproduce the ground state energy of light nuclei and properties of nuclear matter. In particular, the central term was introduced to compensate the overbinding in nuclei and the large equilibrium density of nuclear matter. Their values are $A_{2\pi} = -0.0293$ MeV and $A_R = 0.0048$ MeV.

3.3 Wave functions

As we have seen in the first part of this chapter, the quality of the trial wave function used in VMC is extremely important. The general form for the wave function adopted in nuclear physics is obtained by separating long-range and short-range contributions [44]. This way, we introduce a correlation operator $\mathcal{F}$ acting on a completely antisymmetric wave function $|\Phi\rangle$ that governs the

long-range behavior and possesses the right quantum number for the system.

$$|\psi\rangle = \mathcal{F}|\Phi\rangle = \mathcal{S}\prod_{i<j}^{A}\left[1 + \hat{U}_{ij} + \sum_{k\neq i,j}^{A}\hat{U}_{ijk}\right]\left[\prod_{i<j} f_c(r_{ij})\right]|\Phi(JMTT_3)\rangle\,. \quad (3.30)$$

$\mathcal{S}$ is a symmetrization operator, acting on two- and three-body correlation operators. $f_c(r_{ij})$ is a central, symmetric, and mostly short ranged correlation. The two body [44, 55] correlator is chosen as a sum of radial functions, multiplying the operators in the Argonne v_{18} that give the greater overall contributions:

$$\hat{U}_{ij} = \sum_{p} f^p(r_{ij})\hat{O}^p_{ij}\,, \quad (3.31)$$

$$\hat{O}^p_{ij} = [1, \boldsymbol{\sigma}_i\cdot\boldsymbol{\sigma}_j, S_{ij}]\otimes[1, \boldsymbol{\tau}_i\cdot\boldsymbol{\tau}_j]\,. \quad (3.32)$$

The functions f^p, as well as f_c, only depend on the inter-particle distance r_{ij} and are obtained solving coupled differential equations for the corresponding channel in the two-body potential. They also have the correct asymptotic boundary conditions, when the system is separated into clusters [44].

Similarly, the three-body correlations are included [55] and are proportional to the NNN interaction, as suggested by perturbation theory:

$$\hat{U}_{ijk} = \epsilon\hat{v}_{ijk}\left(\overline{r}_{ij}, \overline{r}_{jk}, \overline{r}_{ki}\right). \quad (3.33)$$

$\bar{r}$ are scaled inter-particle distances, and the parameter ϵ is small and negative.

The long-range part of the wave function is translationally invariant, fully antisymmetric and has quantum numbers $J,\ M,\ T$ and T_z. For light nuclei, $|\Phi\rangle$ is a sum of Slater determinants of single-particle orbitals. The variational wave function presented is usually used in Monte Carlo calculations as a starting point for a propagation in imaginary time, for example in Green Function Monte Carlo and various other flavors of Diffusion Monte Carlo (DMC). The general idea of DMC is based on the formal solution of the many-body, time dependent, Schrödinger equation ($\hbar$=1):

$$i\frac{\partial}{\partial t}|\psi(t)\rangle = \left(\hat{H} - E_T\right)|\psi(t)\rangle \quad \Rightarrow \quad |\psi(t+dt)\rangle = \mathrm{e}^{-i\left(\hat{H}-E_T\right)dt}|\psi(t)\rangle, \tag{3.34}$$

that, using the substitution $\tau = it$, yields

$$|\psi(\tau + d\tau)\rangle = \mathrm{e}^{-\left(\hat{H}-E_T\right)d\tau}|\psi(\tau)\rangle. \tag{3.35}$$

As it is clear using the expansion Eq. (3.8) of the wave function on a complete basis of autostates of $\hat{H}$, the imaginary time evolution of Eq. (3.35) becomes:

$$|\psi(\tau)\rangle = \sum_{n=0}^{\infty} c_n \mathrm{e}^{-(E_n - E_T)\tau}\,|\varphi_n\rangle\,. \tag{3.36}$$

By taking the limit $\tau \to \infty$, excited states are exponentially suppressed, with respect to the ground state. With this method then, one can improve the quality of the ground state wave function by eliminating contributions coming from excited states.

In this work, we will only use variational wave functions, since results for light nuclei [11, 61] suggest that, for electroweak matrix elements, an

$^AZ(J^\pi;T)$	E (MeV)		$\langle r_p^2[r_n^2]\rangle^{1/2}$ (fm)		
	VMC	Expt.	VMC		Expt.
^{2}H$(1^+;0)$	-2.2249(2)	-2.2246	1.966(1)		1.96
^{3}H$(\frac{1}{2}^+;\frac{1}{2})$	-8.26(1)	-8.482	1.611(1)	[1.744(1)]	1.58
^{3}He$(\frac{1}{2}^+;\frac{1}{2})$	-7.52(1)	-7.718	1.770(1)	[1.628(1)]	1.76
^{4}He$(0^+;0)$	-27.55(3)	-28.30	1.444(1)		1.462(6)
^{6}Li$(1^+;0)$	-28.57(3)	-31.99	2.405(5)		2.45(4)

Table 3.1: VMC results for $A \leq 6$ nuclear ground state energies and point radii, compared to experimental values[56–60]. VMC statistical errors and experimental errors are shown in parentheses, errors of less than 1 in the last decimal place are omitted.

additional imaginary time propagation only improves on VMC results at the few percent level. It would be interesting to prove this assumption in future work.

The wave function in Eq. (3.30) can already accurately describe a variety of nuclear properties. In Table 3.1 we give the calculated ground state energies and proton point radii. With the exception of ^{6}Li variational energy, which differs from the experimental value by about 10%, all the other calculated values fall within 2–3% of the experimental value.

Table 3.2 contains the contribution to the total energy of kinetic, two- and three-body potential energy. While these quantities are non-observable, it is useful to consider them when comparing our results with others in the literature, that use different nuclear potentials and wave functions.

$Z(J^\pi;T)$	$\langle T\rangle$	$\langle v_{ij}\rangle$	$\langle v_{ijk}\rangle$
^{2}H$(1^+;0)$	19.80(2)	-22.02(2)	
^{3}H$(\frac{1}{2}^+;\frac{1}{2})$	49.74(5)	-57.01(4)	-0.998(2)
^{3}He$(\frac{1}{2}^+;\frac{1}{2})$	48.95(3)	-55.50(3)	-0.974(3)
^{4}He$(0^+;0)$	110.5(1)	-132.8(2)	-5.26(3)
^{6}Li$(1^+;0)$	148.4(4)	-171.7(4)	-5.29(3)

Table 3.2: VMC expectation values of kinetic, two- and three-body potential energy.

3.4 Cross section and event rate

After introducing the variational Monte Carlo method and the phenomenological potential for the interaction between the nucleons, we can now turn to the computation of experimental observables. We will write the relevant quantities for dark matter direct detection (DD), i.e. the differential cross section for elastic scattering, in terms of matrix elements of the currents derived in Chapter 2, and the differential event rate rate. These quantities are calculated in a non-relativistic regime, since the typical speed of dark matter particles, in our position in the galaxy, is of the order of $v \sim 10^{-3}c$ and the momentum exchanged we consider ranges from 0 to 100 MeV.

For the scalar case we consider, we can express the differential cross section as [62]:

$$\frac{d\sigma}{d\boldsymbol{q}^2} = \frac{1}{4\pi v_\chi^2}\frac{1}{2j+1} \times \sum_{m_j,m'_j=-j}^{j} \left|\langle\psi_{jm'_j}|J(\boldsymbol{q})|\psi_{jm_j}\rangle\right|^2 , \tag{3.37}$$

using matrix elements of the current in Eq. (2.21) for each given nucleus, with a ground state characterized by a total spin j and polarization m_j. We

adopt a non-relativistic state normalization for the DM particle and nucleus. v_χ denotes the velocity of the DM particle.

This cross section can then be used to calculate the differential recoil rate, that can be measured in experiments, and is expressed as (counts per day)/kg/keV:

$$\frac{\mathrm{d}R}{\mathrm{d}E_\mathrm{R}} = \frac{1}{m_N}\frac{\rho_\chi}{m_\chi}\int_{v_\mathrm{min}(E_\mathrm{R})} \mathrm{d}^3\boldsymbol{v}\,|\boldsymbol{v}|\,f_\mathrm{E}(\boldsymbol{v})\frac{\mathrm{d}\sigma}{\mathrm{d}E_\mathrm{R}}\,(v, E_\mathrm{R})\,, \tag{3.38}$$

where ρ_χ is the local DM energy density and $v_\mathrm{min} = \sqrt{m_N E_\mathrm{R}/2\mu^2}$. In principle, there is no upper limit of integration in Eq. (3.38), but in practice it is limited by the escape velocity of DM in our galaxy. An additional assumption needs to be made about the velocity distribution in the Earth's frame $f_\mathrm{E}(\boldsymbol{v})$, where the usual choice is a Maxwell-Boltzmann distribution.

Chapter 4

Results

In this Chapter, we present and expand on the results, already published in [27], for the calculations for the differential cross section and one- and two-body contributions appearing at NLO. Using the VMC method and phenomenological wave functions described in Chapter 3, we study the effects of the currents derived in Chapter 2 on the cross section for scattering of DM particles off the following light nuclei d, ^{3}H, ^{3}He, ^{4}He and ^{6}Li.

The cross section in Eq. (3.37) can be conveniently expanded, as in Ref. [23], as a sum of nuclear response functions $\mathcal{F}_{a,i}^{(\nu)}$. The label ν refers to the chiral order, the label a distinguishes between isoscalar and isovector contributions, and we use the label $i = \{\mathrm{r}, 2\mathrm{b}\}$ for the so-called "nucleon radius" correction and the contributions of two-body currents. The nucleon radius arises in the one-body current at NLO, and gives the momentum-dependent correction in Eq. (2.17), proportional to $F\left(\frac{|\boldsymbol{q}_i|}{2m_\pi}\right)$.

With this choice of nuclear response functions and neglecting the contri-

butions from c_s and c_G, the differential cross section is:

$$\begin{aligned}\frac{d\sigma}{d\boldsymbol{q}^2} &= \frac{c_{\rm is}^2}{\tilde{\Lambda}^6}\frac{\sigma_{\pi N}^2 A^2}{4\pi v_\chi^2}\times \\ &\left|\mathcal{F}_{\rm is}^{(0)}(\boldsymbol{q}^2)+\mathcal{F}_{\rm is,2b}^{(1)}(\boldsymbol{q}^2)+\mathcal{F}_{\rm is,r}^{(1)}(\boldsymbol{q}^2)-\frac{c_{\rm iv}}{c_{\rm is}}\frac{\delta m_N}{4\sigma_{\pi N}}\mathcal{F}_{\rm iv}^{(0)}(\boldsymbol{q}^2)\right|^2 .\end{aligned} \tag{4.1}$$

The isoscalar coupling, the pion nucleon σ term, and the number of nucleons A are factorized in order to have $\mathcal{F}_{\rm is}^{(0)}(0)=1$. At LO, the cross section for the isoscalar case is $\frac{c_{\rm is}^2}{\tilde{\Lambda}^6}\frac{\sigma_{\pi N}^2 A^2}{4\pi v_\chi^2}$, since the scalar current simply counts the number of nucleons.

Without loss of generality, we can focus for the moment on the case $c_{\rm is}\neq 0$ and set $c_{\rm iv,s,G}/c_{\rm is}=0$. These additional couplings do not introduce independent nuclear responses, for the cross section for the general case $c_{\rm iv,s,G}\neq 0$ can be obtained from Eq. (2.17) using

$$\mathcal{F}_{\rm iv}^{(0)}(\boldsymbol{q}^2)=\frac{2Z-A}{A}\times\mathcal{F}_{\rm is}^{(0)}(\boldsymbol{q}^2) \tag{4.2}$$

and rescaling $\mathcal{F}_{\rm is}^{(0)}(\boldsymbol{q}^2)$ in Eq. (4.1) by the factor

$$1+\left(\frac{c_{\rm s}}{c_{\rm is}}\right)\frac{\sigma_s-\dot{\sigma}_s\,\boldsymbol{q}^2}{\sigma_{\pi N}}-\left(\frac{c_G}{c_{\rm is}}\right)\frac{8\pi m_N^G}{9\sigma_{\pi N}} . \tag{4.3}$$

$\dot{\sigma}_s=(0.3\pm 0.2)\text{GeV}^{-2}$ is taken from the dispersive extraction in Ref. [63], as it cannot be obtained in SU2 χPT. The gluon part in Eq. (4.3) contains order (2) contributions, given by $\sigma_{\pi N}$ and σ_s:

$$m_N^G=m_N-\sigma_{\pi N}-\sigma_s. \tag{4.4}$$

In our calculations, we consider the momentum transfer $\boldsymbol{q}$ in the range $0 - 100$ MeV. In the non-relativistic limit, appropriate for a value of local DM velocity $v \sim 10^{-3}c$, the exchanged momentum is limited from above and is given by

$$|\boldsymbol{q}| \leq |\boldsymbol{q}_{\max}| = 2\mu v^{(\mathrm{esc})}\,, \tag{4.5}$$

where $\mu = m_N m_\chi/(m_N + m_\chi)$ is the reduced mass of the DM-nucleus system and $v^{(\mathrm{esc})} \approx 544$ km/s [64] is the escape velocity of DM in our galaxy. Considering a DM particle candidate with a mass $m_\chi \approx 1$ GeV, the maximum momentum transfer ranges from a few to tens of MeV, for the light nuclei we are interested in.

The value of the cutoff Λ applied to regularize the two-body current (see the Appendix A) varies in a range from 500 MeV to 10 GeV, to explore the uncertainty related to the choice of the cutoff.

We will present the results for the differential cross section and, for each nucleus, compare the contribution for $\nu = 0, 1$. The relative contributions of NLO currents are also assessed. While our results do not show the uncertainty related to the σ term and strong proton-neutron mass splitting, we will briefly comment on the effect of these hadronic quantities.

4.1 Cross section

In Fig. 4.1, we show the isoscalar nuclear response function, at LO and NLO, for nuclei from d to ^{6}Li. We consider for the moment the limit of high cutoff Λ for the two-body current. Starting at LO, we can see that the response function is equal to 1, because of the normalization we adopted.

At larger momentum, the response functions decrease. NLO contributions slightly increase the total cross section at low momenta. As $\boldsymbol{q}$ increases, the cross section is reduced, since the contributions from two-body and radius correction are of opposite sign, and the latter is greater. For the isoscalar case, this behavior is consistent for all the nuclei considered here. The results are identical for the nuclei with $A = 3$ and only ^{3}He is shown in Fig. 4.1. The overall effect of NLO contributions is small and accounts for a few percent change of the response functions in the range of momenta considered and for all the nuclei.

Considering the isovector case, in Fig. 4.2 we show the LO contribution, since no contributions appear at NLO. The isovector interaction, at $\boldsymbol{q} = 0$, counts the number of protons minus the number of neutrons. The only nonzero contributions are found in ^{3}H and ^{3}He, and are of opposite sign. Even though the isovector response function seems suppressed by a factor $\delta m_N/4\sigma_{\pi N}$ compared to the isoscalar one, their relative size depends also on the ratio $c_{\rm iv}/c_{\rm is}$ and could easily be enhanced in specific DM models.

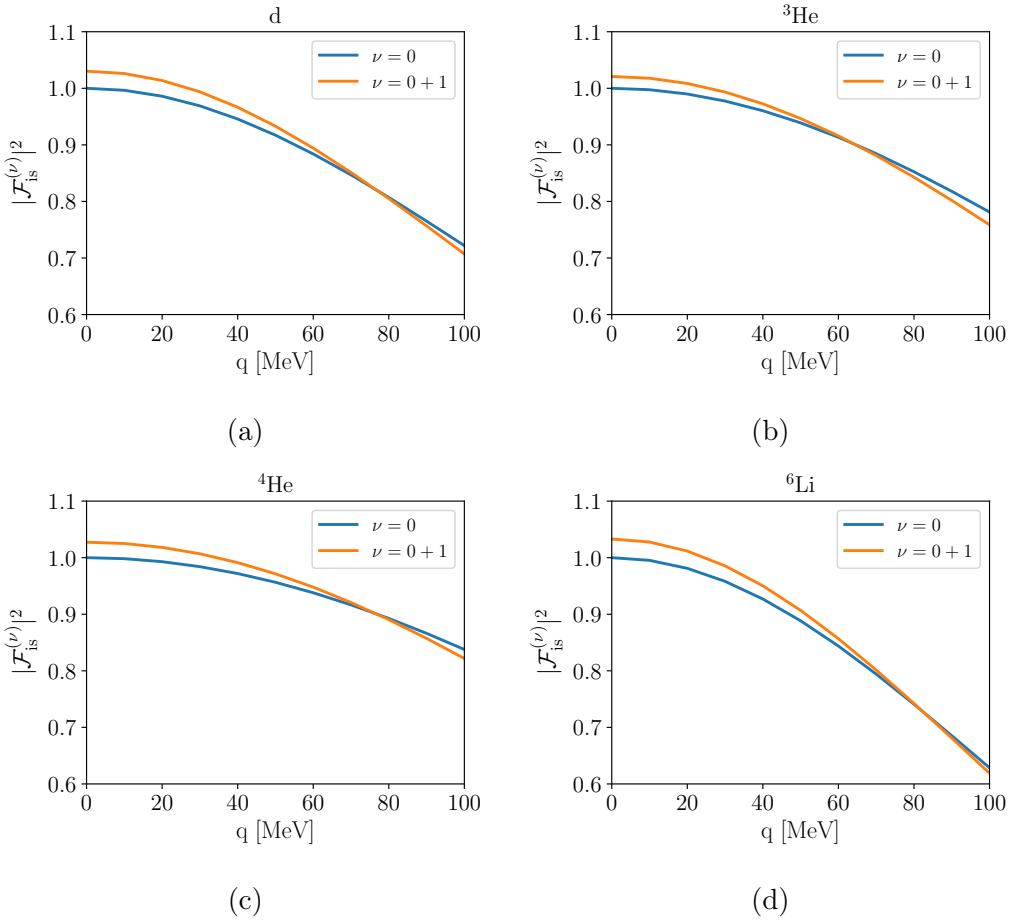

Figure 4.1: Isoscalar response function, for nuclei from A=2 to 6. Dashed blue lines correspond to LO calculations, and orange solid ones correspond to NLO.

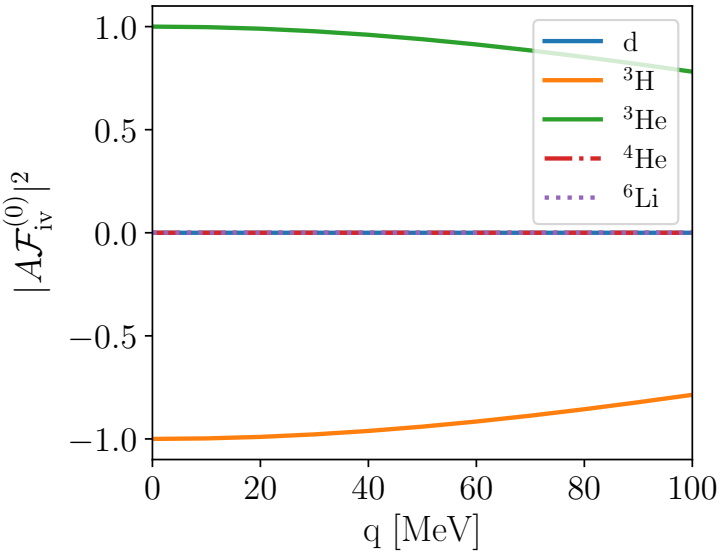

Figure 4.2: Isovector response function, for nuclei from A=2 to 6.

4.2 Radius correction

We now consider the relative contribution to the total cross section, of the one-body current appearing at NLO. We refer to is as radius correction, defined as [23]:

$$\Delta^{(r)} = \frac{\left|\mathcal{F}_{\text{is}}^{(0+1)}(\boldsymbol{q}^2)\right|^2 - \left|\mathcal{F}_{\text{is}}^{(0)}(\boldsymbol{q}^2) + \mathcal{F}_{\text{is,2b}}^{(1)}(\boldsymbol{q}^2)\right|^2}{\left|\mathcal{F}_{\text{is}}^{(0+1)}(\boldsymbol{q}^2)\right|^2}\,, \tag{4.6}$$

where $\mathcal{F}_{\text{is}}^{(0+1)}(\boldsymbol{q}^2)$ is the sum of all the isoscalar terms on the right-hand side of Eq. (4.1). The definition in Eq. (4.6) is a good measure of the relative importance of radius corrections and it captures the percentual contribution of NLO contributions with respect to the total cross section.

Our calculations show only minor difference between the various nuclei, due to the small two-body contribution. In Fig. 4.3 we present the radius correction for ^{4}He, we note that it vanishes at $\boldsymbol{q} = 0$ and grows to about 6% at $\boldsymbol{q} = 100$ MeV.

Comparing our results with [23], we find contributions about three times larger.

Other than the full nuclear calculations, performed with VMC and accurate wave functions, we can derive a simple approximation for Eq. (4.6). Expanding Eq. (4.6) in a Taylor series for small $\mathcal{F}_{\text{is,2b}}^{(1)}(\boldsymbol{q}^2)$ and $\mathcal{F}_{\text{is,r}}^{(1)}(\boldsymbol{q}^2)$ NLO corrections, the expression reduces to

$$\Delta^{(r)} \sim \frac{2\mathcal{F}_{\text{is,r}}^{(1)}(\boldsymbol{q}^2)}{\mathcal{F}_{\text{is}}^{(0+1)}(\boldsymbol{q}^2)} \sim -\frac{2}{\sigma_{\pi N}} \frac{9 g_A^2 \pi m_\pi^3}{4(4\pi f_\pi)^2} F\left(\frac{|\boldsymbol{q}|}{2m_\pi}\right). \tag{4.7}$$

Nuclear effects enter at higher order in the expansion and through the

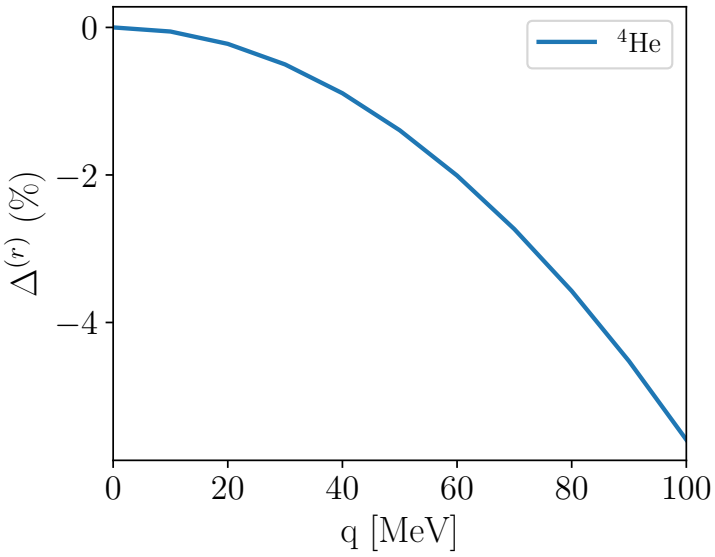

Figure 4.3: Percentual radius correction for ^{4}He.

two-body current, Eq. (4.7) is determined by the momentum dependence of Eq. (2.17). We find Eq. (4.7) in good agreement with the full nuclear calculation, for the value of $\boldsymbol{q}$ considered.

4.3 Two-body contribution

In a similar fashion to Eq. (4.6), we define the relative contribution of two-body currents as [23]:

$$\Delta^{(2b)} = \frac{\left|\mathcal{F}_{\rm is}^{(0+1)}(\boldsymbol{q}^2)\right|^2 - \left|\mathcal{F}_{\rm is}^{(0)}(\boldsymbol{q}^2) + \mathcal{F}_{\rm is,r}^{(1)}(\boldsymbol{q}^2)\right|^2}{\left|\mathcal{F}_{\rm is}^{(0+1)}(\boldsymbol{q}^2)\right|^2}. \tag{4.8}$$

We first consider the case of high cutoff, for the two-body currents. Our results in Fig. 4.4 show that, for all the nuclei considered, two-body contributions are of modest size. They range from about 2% up to about 4%.

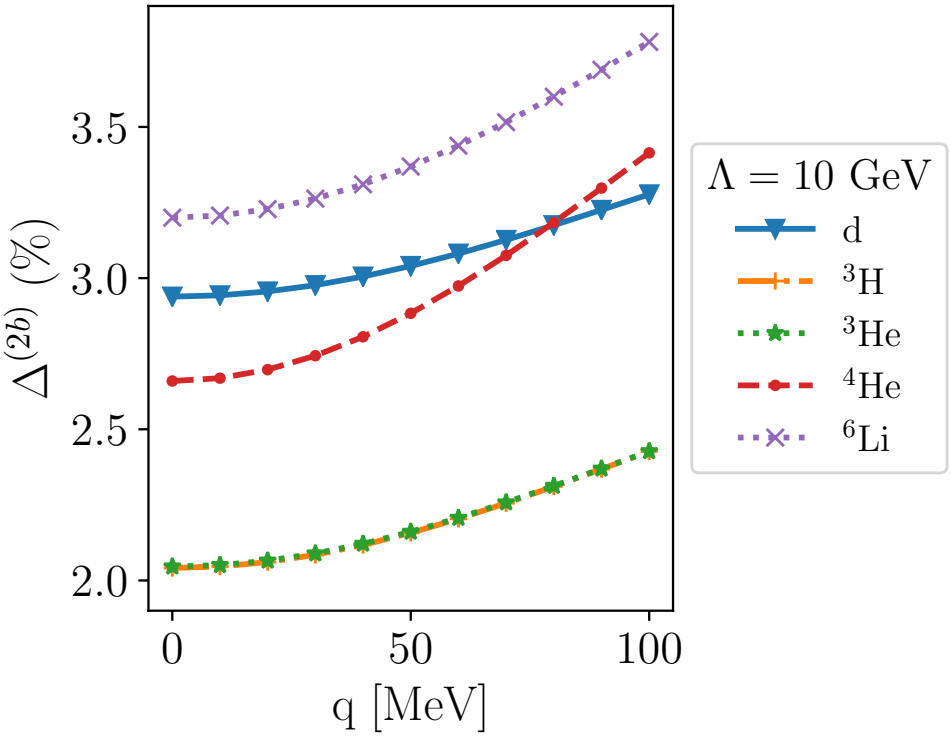

Figure 4.4: Percentual two-body correction to the total cross section for various nuclei, at $\Lambda = 10$ GeV.

As already noted for the total cross section, ^{3}H and ^{3}He give similar results. While the two-body correction generally increases with the exchanged momentum $\boldsymbol{q}$ and the number of nucleons A, d does not follow this trend. The effect of two body currents in d is larger than in $A = 3$ nuclei, a result that is in agreement with what was previously found in [23].

It is important to stress that our results are valid only considering the isoscalar case. Different regions of the parameters space, in the case $c_{\mathrm{iv,s,G}} \neq 0$, can be explored using the rescaling introduced in Eq. (4.3).

So far we only presented calculations for the two-body currents in the

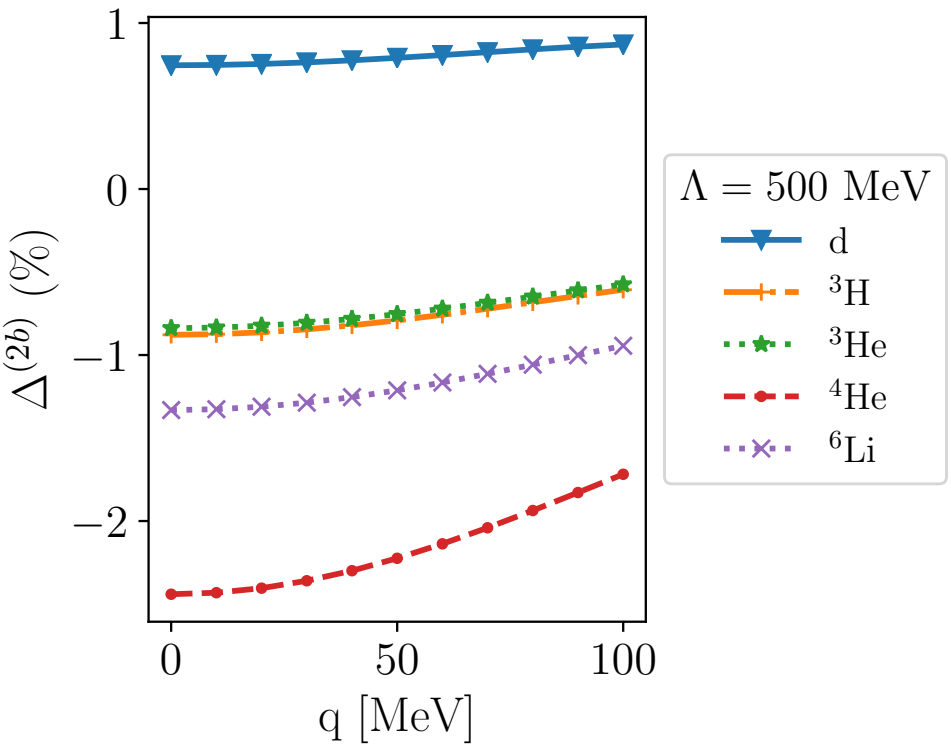

Figure 4.5: Percentual two-body correction to the total cross section for various nuclei, at $\Lambda = 500$ MeV.

limit of infinite cutoff Λ in Eq. (A.3), we now study the effect of the short-distance regulator introduced in the Fourier transforms (see the Appendix) of two-body currents.

In general, to study the dependence of nuclear matrix elements on the cutoff applied to the currents, different approaches are possible. In [23], currents and nuclear wave functions are derived from chiral EFT, so that the same cutoff can be used for both. On the other hand, using phenomenological Hamiltonians, one does not have "strong" low-energy constants that allow for a variation of the cutoff when obtaining the nuclear wave function.

In [11], where an approach similar to the present work was used to perform β-decay calculations, the strategy used was to fix the cutoff in the currents, fit the "weak" low-energy constants in order to reproduce some observable, and predict properties of larger nuclei with $A = 6 - 12$.

However, dealing with scalar mediated DM, up to NLO there are no new low-energy constants in the currents and this approach is not viable. So we study the cutoff dependence of the fractional two-body corrections, simply calculating them for different values of Λ. We show the values of $\Delta^{(2b)}$ as a function of the exchanged momentum, at $\Lambda = 500$ MeV and $\Lambda = 10$ GeV, in Fig. 4.4 and Fig. 4.5, respectively. In Fig. 4.6 we show the two-body contribution for $\boldsymbol{q} = 0$, for a range of values of the cutoff and for all the nuclei considered.

The two-body contributions are strongly dependent on the cutoff, for values up to 1 GeV, and they start to saturate at large values, around 2 GeV. It is possible that this behavior is caused by the hard core of the Argonne v_{18} potential: the "effective" cutoff is very high and could explain the huge variation for low values of Λ.

While for d $\Delta^{(2b)}$ is positive for all values of Λ, the other nuclei change sign as the cutoff increases: at $\Lambda \sim 700$ MeV in $A = 3$ nuclei and ^{6}Li, and at $\Lambda \sim 800$ MeV for ^{4}He. This behavior can be explained by a large cancellation between the operators in Eq. (A.3). At $\boldsymbol{q} = 0$, only two operators give nonzero contributions:

$$\begin{aligned} \mathcal{O}_1 &\sim \boldsymbol{\sigma}_1 \cdot \boldsymbol{\sigma}_2 \,, \\ \mathcal{O}_2 &\sim \boldsymbol{\sigma}_1 \cdot \hat{\boldsymbol{r}}\; \boldsymbol{\sigma}_2 \cdot \hat{\boldsymbol{r}}. \end{aligned} \tag{4.9}$$

In Table 4.1, we give the value of the two contributions, for d and ^{4}He,

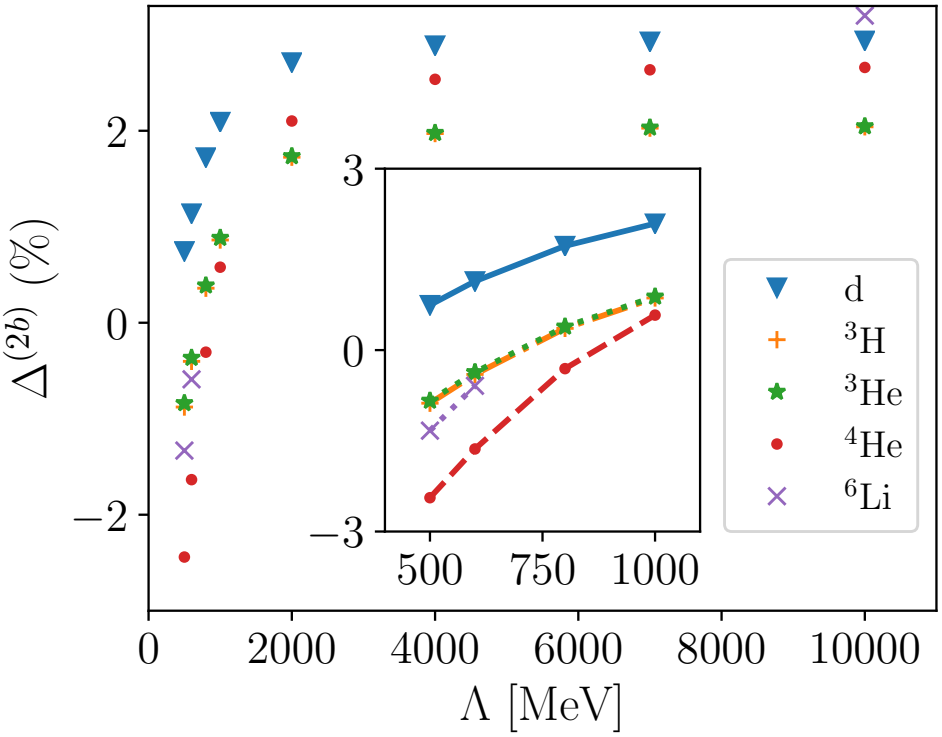

Figure 4.6: Cutoff dependence of the two-body contribution at $\boldsymbol{q} = 0$.

and their sum.

They are of opposite sign and one order of magnitude bigger than their sum, making the total two-body contribution strongly dependent on the choice of the cutoff.

While we presented calculations only for interaction derived in SU(2) χPT, considering SU(3) allows for running of strange heavier mesons in the loop in Fig. 2.2b, and the exchange of two η mesons in Fig. 2.2c. Even though the full calculations is not presented here, we found a suppression caused by the operatorial structure as well as the shorter range of the η-mediated interaction, as in[19]. The two-body contribution in Eq. (4.6) is not altered

Nucleus	Λ [MeV]	$\Delta^{(2b)}$ (%)		
		$\mathcal{O}_1$	$\mathcal{O}_2$	$\mathcal{O}_1 + \mathcal{O}_2$
d	500	-3.4	4.2	0.7
	10000	-4.9	7.9	3.0
^{4}He	500	-13.2	10.7	-2.4
	10000	-19.2	21.9	2.7

Table 4.1: Percentual two-body correction to the total cross section for non-vanishing operators contributing at $\boldsymbol{q} = 0$.

appreciably for natural choices of the coupling of DM to the strange quark; even though one can imagine scenarios in which a combinations of Wilson coefficients leads to an enhancement, they are not addressed here.

In our calculations the statistical uncertainty coming from the Monte Carlo calculations is small, and the biggest source of uncertainty comes from the cutoff dependence in the two-body current. The use of chiral nuclear potential, consistent with one- and two-body currents (in the spirit of [23]), could mitigate the cutoff dependence and help reduce the systematic uncertainty in our results.

In addition to that, more profound reasons could explain the large dependence of the scalar two-body currents on the cutoff. Recent results presented in [65] regarding neutrinoless double-beta decay show the need to introduce, at LO, a short-range operator. This new counterterm is necessary to absorb a divergence in the scattering amplitudes, for the process $nn \to ppee$. The divergence is caused by the neutrino potential part proportional to $1/\boldsymbol{q}^2$, acting on the $^1S_0$ wave.

In the context of this work a counterterm might be need to cure the cutoff dependence, as the two-body current we used has the same scaling of $1/\boldsymbol{q}^2$ in

the limit of large exchanged momentum. A detailed study of the correctness of the power counting used in this work is then certainly warranted, and would shed light on the problematic dependence of our results on the cutoff used.

To conclude, it is also important to note that the choice of the value for the nucleon σ term affects the relative size of NLO correction with respect to the LO. In this work, we used a value taken from a Roy-Steiner analysis of pion-nucleon scattering [40], however, smaller values have been found in recent lattice-QCD calculations. For example, using the value in [42] would increase the relative size of NLO contributions, as is clear from Eq. (2.17) and Eq. (2.20), together with the factorization adopted in the total cross section.

Chapter 5

Conclusions and outlook

5.1 Conclusions

In this work, we have studied the cross section for elastic scattering of dark matter particles, off a variety of light nuclei (d, ^{3}H, ^{3}He, ^{4}He, and ^{6}Li). The nuclei under consideration, up to $A = 6$, present a variety of spin and isospin structure. This study is motivated by the growing interest in light nuclei as targets in DM direct detection experiments, and by the role played by two-body currents.

Our calculations, performed using quantum Monte Carlo methods, followed a hybrid approach. The ground state nuclear wave functions are obtained from a phenomenological Hamiltonian composed of two- and three-body nuclear interactions, the Argonne v_{18} and Urbana IX, respectively. The interaction between DM and nucleons is derived in the context of chiral perturbation theory, up to NLO, starting from a scalar effective Lagrangian for DM-quark and DM-gluons, parameterized by four Wilson coefficients.

Restricting the calculations to exchanged momenta up to 100 MeV, appropriate for the nuclei considered, we have studied the effect of the NLO contributions to the differential cross section, considering both the nucleon "scalar radius" and two-body currents.

We find that their size is smaller than what suggested by chiral power counting, and is at the few percent level. In particular, the nucleon scalar radius correction is zero at $q = 0$, approximately -2% at $q = 60$ MeV and -6% at $q = 100$ MeV. This results is equivalent for all the nuclei considered and does not suffer from uncertainties due to the nuclear structure calculations. Our results can be compared to Ref. [66], when considering only the one-body current (corresponding to the operator $\hat{\mathcal{O}}_1$ in the NREFT basis of Ref. [26]). Our results are in good qualitative agreement, for ^{3}He and ^{4}He.
The two-body currents give a contribution of 2–3% at $q = 0$ for all the nuclei considered, and slightly grow with q. We find a qualitative agreement with [23] in the cases of $A = 2$ and $A = 3$, and we give for the first time an estimate of their contribution in systems with $A = 4$ and $A = 6$.

The two-body current has an uncertainty associated with the variation of the cutoff. Even considering values of the cutoff between $\Lambda = 500$ MeV and $\Lambda = 2$ GeV, we can determine the differential cross section with an accuracy of a few percent. Our results, together with Refs. [23, 66], are already relevant for the assessment of the sensitivity in future experimental searches.

5.2 Outlook

This work is based on a hybrid approach and uses a phenomenological Hamiltonian for NN and NNN interactions, while using chiral currents for the DM-nucleon interaction. It would certainly be interesting to perform fully consistent calculations, using a chiral nuclear potential to obtain the nuclear wave functions. This would allow for a variation of the cutoff, both for ground state wave functions and two-body currents.

Quantum Monte Carlo methods based on the VMC and additional propagation in imaginary time of the wave function, allow performing calculations for medium-heavy nuclei. Calculations for such nuclei would be interesting in assessing the size of two-body currents as the dimension of the system grows.

While not addressed in this work, it is worth studying the applicability of Weinberg power counting for the various channels of DM-nucleon two-body, as briefly mentioned in Chapter 4.

Finally, it would be interesting to explore the connection between our results and lattice QCD calculations [28, 29]. Recent results suggest that the cross section for scalar interaction in light nuclei is affected by meson-exchange currents only at the few percent level [29], in agreement with the present work.

Appendices

Appendix A

Fourier Transforms

A.1 Scalar

We perform QMC calculations in coordinate space, so we need to Fourier transform the one- and two-body DM-nucleon currents we presented in Chapter 2. While transforming the currents, we introduce a Gaussian regulator with cutoff parameter Λ, to tame the short-distance singularities:

$$S_\Lambda(\boldsymbol{k}^2) = e^{-\frac{\boldsymbol{k}^2}{2\Lambda^2}} \ . \tag{A.1}$$

The two-body current is then obtained from

$$\begin{aligned} J^{(2)}_{\pi\pi}(\boldsymbol{q};\boldsymbol{r}_1,\boldsymbol{r}_2) = \int \frac{d^3\boldsymbol{k}_1}{(2\pi)^3}\frac{d^3\boldsymbol{k}_2}{(2\pi)^3} e^{i\boldsymbol{k}_1\cdot\boldsymbol{r}_1} e^{i\boldsymbol{k}_2\cdot\boldsymbol{r}_2} S_\Lambda(\boldsymbol{k}_1^2) S_\Lambda(\boldsymbol{k}_2^2) \\ \times (2\pi)^3\delta^{(3)}(\boldsymbol{k}_1+\boldsymbol{k}_2-\boldsymbol{q}) J^{(2)}_{\pi\pi}(\boldsymbol{k}_1,\boldsymbol{k}_2). \end{aligned} \tag{A.2}$$

This integration can be performed analitically, with the exception of one

integration over an auxiliary variable y. The coordinate space expression for the two-body current in coordinate space reads

$$\begin{aligned} J^{(2)}_{\pi\pi}(\boldsymbol{q};\boldsymbol{r}_1,\boldsymbol{r}_2) = &-\frac{1}{\Lambda^3}\left(\frac{g_A}{2F_\pi}\right)^2 c_{\rm is} m_\pi^2 \boldsymbol{\tau}_1\cdot\boldsymbol{\tau}_2 \frac{1}{2} e^{i\boldsymbol{q}\cdot\boldsymbol{R}} \int_{-1}^{1} dy e^{-i\boldsymbol{q}\cdot\boldsymbol{r}y/2} \\ &\times\Bigg[(\boldsymbol{\sigma}_1\cdot\boldsymbol{q})(\boldsymbol{\sigma}_2\cdot\boldsymbol{q})\frac{1-y^2}{4}s(r,y) + (\boldsymbol{\sigma}_1\cdot\boldsymbol{q})(\boldsymbol{\sigma}_2\cdot\hat{\boldsymbol{r}})\left(-i\frac{1+y}{2}\right)\frac{\partial}{\partial r}s(r,y) \\ &\quad + (\boldsymbol{\sigma}_1\cdot\hat{\boldsymbol{r}})(\boldsymbol{\sigma}_2\cdot\boldsymbol{q})\left(i\frac{1-y}{2}\right)\frac{\partial}{\partial r}s(r,y) + (\boldsymbol{\sigma}_1\cdot\boldsymbol{\sigma}_2)\frac{1}{r}\frac{\partial}{\partial r}s(r,y) \\ &\quad + (\boldsymbol{\sigma}_1\cdot\hat{\boldsymbol{r}})(\boldsymbol{\sigma}_2\cdot\hat{\boldsymbol{r}})r\frac{\partial}{\partial r}\frac{1}{r}\frac{\partial}{\partial r}s(r,y)\Bigg], \end{aligned} \tag{A.3}$$

where $\boldsymbol{r} = \boldsymbol{r}_2 - \boldsymbol{r}_1$, $\boldsymbol{R} = \frac{\boldsymbol{r}_2+\boldsymbol{r}_1}{2}$, and the radial functions have the following expressions:

$$s(r,y) = \frac{e^{L^2/\Lambda^2}}{8\pi L\Lambda r}\left[\mathrm{erfc}\left(\frac{L}{\Lambda}+\frac{\Lambda r}{2}\right)e^{Lr}\left(\frac{L}{\Lambda}+\frac{\Lambda r}{2}\right) - \mathrm{erfc}\left(\frac{L}{\Lambda}-\frac{\Lambda r}{2}\right)e^{-Lr}\left(\frac{L}{\Lambda}-\frac{\Lambda r}{2}\right)\right], \tag{A.4}$$

$$\begin{aligned} \frac{\partial}{\partial r}s(r,y) = &\frac{e^{L^2/\Lambda^2}}{8\pi\Lambda^2 r^2}\Bigg[\mathrm{erfc}\left(\frac{L}{\Lambda}+\frac{\Lambda r}{2}\right)e^{Lr}\left(-1+Lr+\frac{\Lambda^2 r^2}{2}\right) \\ &+ \mathrm{erfc}\left(\frac{L}{\Lambda}-\frac{\Lambda r}{2}\right)e^{-Lr}\left(1+Lr-\frac{\Lambda^2 r^2}{2}\right)\Bigg] - \frac{e^{-\Lambda^2 r^2/4}}{4\pi^{3/2}\Lambda r}, \end{aligned} \tag{A.5}$$

$$
\begin{aligned}
r\frac{\partial}{\partial r}\frac{1}{r}\frac{\partial}{\partial r}s(r,y) =& \frac{e^{L^2/\Lambda^2}}{8\pi\Lambda^2 r^3}\left[\operatorname{erfc}\left(\frac{L}{\Lambda}+\frac{\Lambda r}{2}\right)e^{Lr}\left(3-3Lr+L^2r^2-\frac{\Lambda^2r^2}{2}+\frac{Lr\Lambda^2r^2}{2}\right)\right.\\
&\left.+\operatorname{erfc}\left(\frac{L}{\Lambda}-\frac{\Lambda r}{2}\right)e^{-Lr}\left(-3-3Lr-L^2r^2+\frac{\Lambda^2r^2}{2}+\frac{Lr\Lambda^2r^2}{2}\right)\right]\\
&+\frac{3e^{-\Lambda^2r^2/4}}{4\pi^{3/2}\Lambda r^2},
\end{aligned}
\tag{A.6}
$$

$$
\begin{aligned}
r^2\frac{\partial}{\partial r}\frac{1}{r}\frac{\partial}{\partial r}\frac{1}{r}\frac{\partial}{\partial r}s(r,y) =& \frac{e^{L^2/\Lambda^2}}{8\pi\Lambda^2 r^4}\\
&\times\left[\operatorname{erfc}\left(\frac{L}{\Lambda}+\frac{\Lambda r}{2}\right)e^{Lr}\left(-10+10Lr-5L^2r^2+L^3r^3-Lr\Lambda^2r^2+\frac{L^2r^2\Lambda^2r^2}{2}\right)\right.\\
&\left.+\operatorname{erfc}\left(\frac{L}{\Lambda}-\frac{\Lambda r}{2}\right)e^{-Lr}\left(10+10Lr+5L^2r^2+L^3r^3-Lr\Lambda^2r^2-\frac{L^2r^2\Lambda^2r^2}{2}\right)\right]\\
&-\frac{e^{-\Lambda^2r^2/4}(10+L^2r^2+\Lambda^2r^2)}{4\pi^{3/2}\Lambda r^3},
\end{aligned}
\tag{A.7}
$$

$$
L(\boldsymbol{q};y) = \sqrt{m^2+(1-y^2)\frac{\boldsymbol{q}^2}{4}}. \tag{A.8}
$$

In the limit of $\Lambda\to\infty$ the radial functions reduce to

$$
s(r,y) = \frac{e^{-Lr}}{8\pi L}, \tag{A.9}
$$

$$
\frac{\partial}{\partial r}s(r,y) = -\frac{e^{-Lr}}{8\pi}, \tag{A.10}
$$

$$r\frac{\partial}{\partial r}\frac{1}{r}\frac{\partial}{\partial r}s(r,y)=\frac{e^{-Lr}(1+Lr)}{8\pi r}, \tag{A.11}$$

$$r^2\frac{\partial}{\partial r}\frac{1}{r}\frac{\partial}{\partial r}\frac{1}{r}\frac{\partial}{\partial r}s(r,y)=-\frac{e^{-Lr}L(2+Lr)}{8\pi r}. \tag{A.12}$$

In the limit of $\Lambda\to\infty$ and $\boldsymbol{q}=0$, in the above expressions, $L(\boldsymbol{q};y)\to m$.

We can see that the expression reduces to Eqs. (5.8) and (5.9) in Ref. [19] by taking the limit of $\boldsymbol{q}=0$ and $\Lambda\to\infty$ in the above expression, that correctly reduces to

$$\frac{1}{8\pi r}\left[(\boldsymbol{\sigma}_1\cdot\hat{\boldsymbol{r}})(\boldsymbol{\sigma}_2\cdot\hat{\boldsymbol{r}})(1+mr)-(\boldsymbol{\sigma}_1\cdot\boldsymbol{\sigma}_2)\right]e^{-mr}\ . \tag{A.13}$$

Bibliography

[1] "First direct evidence of cosmic inflation," `https://www.cfa.harvard.edu/news/2014-05`, retrieved March 2019.

[2] G. Bertone and D. Hooper, "History of dark matter," Rev. Mod. Phys. **90**, 045002 (2018).

[3] L. Roszkowski, E. M. Sessolo, and S. Trojanowski, "WIMP dark matter candidates and searches—current status and future prospects," Reports on Progress in Physics **81**, 066201 (2018).

[4] M. Battaglieri et al., "US Cosmic Visions: New Ideas in Dark Matter 2017: Community Report," (2017), arXiv:1707.04591 [hep-ph] .

[5] W. Guo and D. N. McKinsey, "Concept for a dark matter detector using liquid helium-4," Phys. Rev. D **87**, 115001 (2013).

[6] T. M. Ito and G. M. Seidel, "Scintillation of liquid helium for low-energy nuclear recoils," Phys. Rev. C **88**, 025805 (2013).

[7] G. Gerbier et al., "NEWS : a new spherical gas detector for very low mass WIMP detection," (2014), arXiv:1401.7902 [astro-ph.IM] .

[8] S. Profumo, "Gev dark matter searches with the news detector," Phys. Rev. D **93**, 055036 (2016).

[9] S. A. Hertel, A. Biekert, J. Lin, V. Velan, and D. N. McKinsey, "A Path to the Direct Detection of sub-GeV Dark Matter Using Calorimetric Readout of a Superfluid ^{4}He Target," (2018), arXiv:1810.06283 [physics.ins-det] .

[10] F. Mayet et al., "A review of the discovery reach of directional Dark Matter detection," Phys. Rept. **627**, 1 (2016), arXiv:1602.03781 [astro-ph.CO] .

[11] S. Pastore, A. Baroni, J. Carlson, S. Gandolfi, S. C. Pieper, R. Schiavilla, and R. B. Wiringa, "Quantum Monte Carlo calculations of weak transitions in $A = 6 - -10$ nuclei," Phys. Rev. C **97**, 022501 (2018).

[12] A. Lovato, S. Gandolfi, R. Butler, J. Carlson, E. Lusk, S. C. Pieper, and R. Schiavilla, "Charge form factor and sum rules of electromagnetic response functions in ^{12}**C**," Phys. Rev. Lett. **111**, 092501 (2013).

[13] A. Lovato, S. Gandolfi, J. Carlson, S. C. Pieper, and R. Schiavilla, "Electromagnetic response of ^{12}C: A first-principles calculation," Phys. Rev. Lett. **117**, 082501 (2016).

[14] A. Lovato, S. Gandolfi, J. Carlson, S. C. Pieper, and R. Schiavilla, "Neutral weak current two-body contributions in inclusive scattering from ^{12}C," Phys. Rev. Lett. **112**, 182502 (2014).

[15] D. Clowe, M. Bradac, A. H. Gonzalez, M. Markevitch, S. W. Randall,

C. Jones, and D. Zaritsky, "A direct empirical proof of the existence of dark matter," Astrophys. J. **648**, L109 (2006).

[16] N. Aghanim et al. (Planck), "Planck 2018 results. VI. Cosmological parameters," (2018), arXiv:1807.06209 [astro-ph.CO] .

[17] Tanabashi et al. (Particle Data Group), "Review of particle physics," Phys. Rev. D **98**, 030001 (2018).

[18] G. Prezeau, A. Kurylov, M. Kamionkowski, and P. Vogel, "New contribution to wimp-nucleus scattering," Phys. Rev. Lett. **91**, 231301 (2003).

[19] V. Cirigliano, M. L. Graesser, and G. Ovanesyan, "Wimp-nucleus scattering in chiral effective theory," JHEP **2012**, 25 (2012).

[20] J. Menéndez, D. Gazit, and A. Schwenk, "Spin-dependent wimp scattering off nuclei," Phys. Rev. D **86**, 103511 (2012).

[21] M. Hoferichter, P. Klos, and A. Schwenk, "Chiral power counting of one- and two-body currents in direct detection of dark matter," Phys. Lett. B **746**, 410 (2015).

[22] M. Hoferichter, P. Klos, J. Menéndez, and A. Schwenk, "Analysis strategies for general spin-independent wimp-nucleus scattering," Phys. Rev. D **94**, 063505 (2016).

[23] C. Körber, A. Nogga, and J. de Vries, "First-principle calculations of dark matter scattering off light nuclei," Phys. Rev. C **96**, 035805 (2017).

[24] F. Bishara, J. Brod, B. Grinstein, and J. Zupan, "From quarks to nucleons in dark matter direct detection," JHEP **11**, 059 (2017).

[25] J. Fan, M. Reece, and L.-T. Wang, "Non-relativistic effective theory of dark matter direct detection," J. Cosmol. Astropart. Phys. **1011**, 042 (2010).

[26] A. L. Fitzpatrick, W. Haxton, E. Katz, N. Lubbers, and Y. Xu, "The Effective Field Theory of Dark Matter Direct Detection," J. Cosmol. Astropart. Phys. **1302**, 004 (2013).

[27] L. Andreoli, V. Cirigliano, S. Gandolfi, and F. Pederiva, "Quantum Monte Carlo calculations of dark matter scattering off light nuclei," Phys. Rev. C **99**, 025501 (2019).

[28] E. Chang, Z. Davoudi, W. Detmold, A. S. Gambhir, K. Orginos, M. J. Savage, P. E. Shanahan, M. L. Wagman, and F. Winter (NPLQCD Collaboration), "Scalar, axial, and tensor interactions of light nuclei from lattice qcd," Phys. Rev. Lett. **120**, 152002 (2018).

[29] S. R. Beane, S. D. Cohen, W. Detmold, H.-W. Lin, and M. J. Savage, "Nuclear σ terms and scalar-isoscalar wimp-nucleus interactions from lattice qcd," Phys. Rev. D **89**, 074505 (2014).

[30] J. Goodman, M. Ibe, A. Rajaraman, W. Shepherd, T. M. P. Tait, and H.-B. Yu, "Gamma ray line constraints on effective theories of dark matter," Nuclear Physics B **844**, 55 (2011), arXiv:1009.0008 [hep-ph] .

[31] J. Brod, A. Gootjes-Dreesbach, M. Tammaro, and J. Zupan, "Effective field theory for dark matter direct detection up to dimension seven," Journal of High Energy Physics **10**, 65 (2018), arXiv:1710.10218 [hep-ph] .

[32] J. Engel, S. Pittel, and P. Vogel, "Nuclear physics of dark matter detection," Int. J. Mod. Phys. **E1**, 1 (1992).

[33] S. Weinberg, "Phenomenological lagrangians," Physica A: Statistical Mechanics and its Applications **96**, 327 (1979).

[34] J. Gasser and H. Leutwyler, "Chiral perturbation theory to one loop," Annals of Physics **158**, 142 (1984).

[35] J. Gasser and H. Leutwyler, "Chiral perturbation theory: Expansions in the mass of the strange quark," Nuclear Physics B **250**, 465 (1985).

[36] A. Crivellin, M. Hoferichter, and M. Procura, "Accurate evaluation of hadronic uncertainties in spin-independent wimp-nucleon scattering: Disentangling two- and three-flavor effects," Phys. Rev. D **89**, 054021 (2014).

[37] S. Weinberg, "Nuclear forces from chiral lagrangians," Physics Letters B **251**, 288 (1990).

[38] S. Weinberg, "Effective chiral lagrangians for nucleon-pion interactions and nuclear forces," Nuclear Physics B **363**, 3 (1991).

[39] D. B. Kaplan, M. J. Savage, and M. B. Wise, "Nucleon-nucleon scattering from effective field theory," Nuclear Physics B **478**, 629 (1996).

[40] M. Hoferichter, J. Ruiz de Elvira, B. Kubis, and U.-G. Meißner, "High-precision determination of the pion-nucleon σ term from roy-steiner equations," Phys. Rev. Lett. **115**, 092301 (2015).

[41] D. A. Brantley, B. Joo, E. V. Mastropas, E. Mereghetti, H. Monge-Camacho, B. C. Tiburzi, and A. Walker-Loud, "Strong isospin violation and chiral logarithms in the baryon spectrum," (2016), arXiv:1612.07733 [hep-lat] .

[42] P. E. Shanahan, "Chiral effective theory methods and their application to the structure of hadrons from lattice QCD," Journal of Physics G: Nuclear and Particle Physics **43**, 124001 (2016).

[43] P. Klos, J. Menéndez, D. Gazit, and A. Schwenk, "Large-scale nuclear structure calculations for spin-dependent wimp scattering with chiral effective field theory currents," Phys. Rev. D **88**, 083516 (2013).

[44] J. Carlson, S. Gandolfi, F. Pederiva, S. C. Pieper, R. Schiavilla, K. E. Schmidt, and R. B. Wiringa, "Quantum Monte Carlo methods for nuclear physics," Rev. Mod. Phys. **87**, 1067 (2015).

[45] J. E. Lynn, I. Tews, J. Carlson, S. Gandolfi, A. Gezerlis, K. E. Schmidt, and A. Schwenk, "Chiral three-nucleon interactions in light nuclei, neutron-α scattering, and neutron matter," Phys. Rev. Lett. **116**, 062501 (2016).

[46] D. Lonardoni, J. Carlson, S. Gandolfi, J. E. Lynn, K. E. Schmidt, A. Schwenk, and X. B. Wang, "Properties of nuclei up to $a = 16$ using local chiral interactions," Phys. Rev. Lett. **120**, 122502 (2018).

[47] P. Billingsley, Probability and Measure, 3rd ed. (John Wiley and Sons, 1995).

[48] N. Metropolis, A. W. Rosenbluth, M. N. Rosenbluth, A. H. Teller, and E. Teller, "Equation of state calculations by fast computing machines," The Journal of Chemical Physics **21**, 1087 (1953).

[49] R. B. Wiringa, V. G. J. Stoks, and R. Schiavilla, "Accurate nucleon-nucleon potential with charge-independence breaking," Phys. Rev. C **51**, 38 (1995).

[50] B. S. Pudliner, V. R. Pandharipande, J. Carlson, S. C. Pieper, and R. B. Wiringa, "Quantum Monte Carlo calculations of nuclei with $A \sim 7$," Phys. Rev. C **56**, 1720 (1997).

[51] J. R. Bergervoet, P. C. van Campen, R. A. M. Klomp, J.-L. de Kok, T. A. Rijken, V. G. J. Stoks, and J. J. de Swart, "Phase shift analysis of all proton-proton scattering data below $T_{\rm lab}$=350 MeV," Phys. Rev. C **41**, 1435 (1990).

[52] V. G. J. Stoks, R. A. M. Klomp, M. C. M. Rentmeester, and J. J. de Swart, "Partial-wave analysis of all nucleon-nucleon scattering data below 350 MeV," Phys. Rev. C **48**, 792 (1993).

[53] J. Carlson, V. Pandharipande, and R. Wiringa, "Three-nucleon interaction in 3-, 4- and -body systems," Nuclear Physics A **401**, 59 (1983).

[54] J. Fujita and H. Miyazawa, "Pion Theory of Three-Body Forces," Progress of Theoretical Physics **17**, 360 (1957).

[55] S. C. Pieper and R. B. Wiringa, "Quantum Monte Carlo calculations

of light nuclei," Annual Review of Nuclear and Particle Science **51**, 53 (2001).

[56] A. Amroun, V. Breton, J.-M. Cavedon, B. Frois, D. Goutte, F. Juster, P. Leconte, J. Martino, Y. Mizuno, X.-H. Phan, S. Platchkov, I. Sick, and S. Williamson, "3h and 3he electromagnetic form factors," Nuclear Physics A **579**, 596 (1994).

[57] D. Shiner, R. Dixson, and V. Vedantham, "Three-nucleon charge radius: A precise laser determination using ^{3}he," Phys. Rev. Lett. **74**, 3553 (1995).

[58] D. Tilley, C. Cheves, J. Godwin, G. Hale, H. Hofmann, J. Kelley, C. Sheu, and H. Weller, "Energy levels of light nuclei a=5, 6, 7," Nuclear Physics A **708**, 3 (2002).

[59] G. Audi, A. Wapstra, and C. Thibault, "The ame2003 atomic mass evaluation: (ii). tables, graphs and references," Nuclear Physics A **729**, 337 (2003), the 2003 NUBASE and Atomic Mass Evaluations.

[60] J. Purcell, J. Kelley, E. Kwan, C. Sheu, and H. Weller, "Energy levels of light nuclei a=3," Nuclear Physics A **848**, 1 (2010).

[61] S. Pastore, S. C. Pieper, R. Schiavilla, and R. B. Wiringa, "Quantum Monte Carlo calculations of electromagnetic moments and transitions in $A \leq 9$ nuclei with meson-exchange currents derived from chiral effective field theory," Phys. Rev. C **87**, 035503 (2013).

[62] M. Cirelli, E. D. Nobile, and P. Panci, "Tools for model-independent

bounds in direct dark matter searches," Journal of Cosmology and Astroparticle Physics **2013**, 019 (2013).

[63] M. Hoferichter, C. Ditsche, B. Kubis, and U. G. Meissner, "Dispersive analysis of the scalar form factor of the nucleon," JHEP **06**, 063 (2012), arXiv:1204.6251 [hep-ph] .

[64] Helmi et al., "The RAVE survey: constraining the local Galactic escape speed," Monthly Notices of the Royal Astronomical Society **379**, 755 (2007).

[65] V. Cirigliano, W. Dekens, J. de Vries, M. L. Graesser, E. Mereghetti, S. Pastore, and U. van Kolck, "New Leading Contribution to Neutrinoless Double-β Decay," Physical Review Letters **120**, 202001 (2018), arXiv:1802.10097 [hep-ph] .

[66] D. Gazda, R. Catena, and C. Forssen, "Ab initio nuclear response functions for dark matter searches," Phys. Rev. **D95**, 103011 (2017).

Acknowledgments

I would first like to thank my advisor, Francesco Pederiva, for its guidance and encouragement, his patience and the many opportunities he has given me in the past years. I will always be grateful to him on a scientific and personal level. I would also like to thank Stefano Gandolfi and Vincenzo Cirigliano for giving me the chance of collaborating with them at Los Alamos National Laboratory, and for their tireless support and advice that helped me get through hard times. I am grateful to the T Division and Joe Carlson, for the great working environment I found at LANL. I am also grateful to the administrative staff in Trento, in particular, Micaela.

I owe a lot to the people I was lucky to meet in New Mexico, in the past years. I would like to mention Diego and his beautiful family, Daniele, Francesco and Edith, Carlos. Francesca, a great friend and the perfect companion.

Special thanks go to the important people in my life.
Ivo, for your friendship and advice, the moment I needed it the most. Enrico and Luisa, for being there all the way, even from afar. Memo and Lalo, I'm happy you're part of my life. Ilaria, Dante, Lorenzo, Paolo, Michele, Daniela, Andrea, Luca.

All my friends from Artogne, you always make me feel like I belong, no matter how long I've been away from home.

Finally, the biggest thank goes to my family, for their unconditional love and support.